JGR Oceans

RESEARCH ARTICLE
10.1029/2022JC019413

The Agulhas Current Transports Signals of Local and Remote Indian Ocean Nitrogen Cycling

Tanya A. Marshall[1], Daniel M. Sigman[2], Lisa M. Beal[3], Alan Foreman[4], Alfredo Martínez-García[4], Stéphane Blain[5], Ethan Campbell[6], François Fripiat[7], Robyn Granger[1], Eesaa Harris[1], Gerald H. Haug[3], Dario Marconi[2], Sergey Oleynik[2], Patrick A. Rafter[8], Raymond Roman[1], Kolisa Sinyanya[1], Sandi M. Smart[1,9], and Sarah E. Fawcett[1,10]

[1]Department of Oceanography, University of Cape Town, Cape Town, South Africa, [2]Department of Geosciences, Princeton University, Princeton, NJ, USA, [3]Rosenstiel School of Marine and Atmospheric Science, University of Miami, Miami, FL, USA, [4]Department of Climate Geochemistry, Max Planck Institute for Chemistry, Mainz, Germany, [5]Laboratoire d'Océanographie Microbienne, Sorbonne Université, Banyuls sur mer, France, [6]School of Oceanography, University of Washington, Seattle, WA, USA, [7]Department of Geosciences, Environment and Society, Université Libre de Bruxelles, Brussels, Belgium, [8]Department of Earth System Science, University of California, Irvine, CA, USA, [9]Department of Geological Sciences, University of Alabama, Tuscaloosa, AL, USA, [10]Marine and Antarctic Research Centre for Innovation and Sustainability and (MARIS), University of Cape Town, Western Cape, South Africa

Abstract The greater Agulhas Current region is an important component of the climate system, yet its influence on carbon and nutrient cycling is poorly understood. Here, we use nitrate isotopes ($\delta^{15}N$, $\delta^{18}O$, $\Delta(15–18) = \delta^{15}N–\delta^{18}O$) to trace regional water mass circulation and investigate nitrogen cycling in the Agulhas Current and adjacent recirculating waters. The deep and intermediate waters record processes occurring remotely, including partial nitrate assimilation in the Southern Ocean and denitrification in the Arabian Sea. In the thermocline and surface, tropically sourced waters are biogeochemically distinct from adjacent subtropically sourced waters, confirming inhibited lateral mixing across the current core. (Sub)tropical thermocline nitrate $\delta^{15}N$ is lower (4.9–5.8‰) than the sub-thermocline source, Subantarctic Mode Water (6.9‰); we attribute this difference to local N_2 fixation. Using a one-box model to simulate the newly fixed nitrate flux, we estimate a local N_2 fixation rate of 7–25 Tg N.a^{-1}, with the upper limit likely biased high. In the mixed layer, nitrate $\delta^{15}N$ and $\delta^{18}O$ rise in unison, indicating that phytoplankton nitrate assimilation dominates in surface waters, with nitrification restricted to deeper waters. Because nitrate assimilation and nitrification are vertically decoupled, the rate of nitrate assimilation plus N_2 fixation can be used to approximate carbon export. Thermocline and mixed-layer nitrate $\Delta(15–18)$ is low, due to both N_2 fixation and coupled partial nitrate assimilation and nitrification. Similarly low-$\Delta(15–18)$ nitrate in Agulhas rings indicates leakage of low-$\delta^{15}N$ nitrogen into the South Atlantic, which should be recorded in the organic matter sinking to the seafloor, providing a potential tracer of past Agulhas leakage.

Plain Language Summary The Agulhas Current is known to transport heat and salt from the warm tropics to the cooler (sub-)polar regions, but little is known of its nutrient fluxes. Here we use new measurements of the essential phytoplankton nutrient, nitrate, and its isotope ratios to better characterize water circulation and the nitrogen cycle in the Agulhas Current and adjacent waters. Below 500 m, we see evidence of processes that occurred in other ocean basins. Above 500 m, we find that the nearby tropical and subtropical waters that feed the current have different chemistries and do not mix across its fast-flowing core. In the sunlit surface layer, the dominant nitrogen cycle process is nitrate uptake by phytoplankton, while nitrification, which produces nitrate from organic matter, occurs only in the dark waters below the surface. Additionally, the Agulhas Current and adjacent waters host significant rates of N_2 fixation, the process by which atmospheric N_2 gas is converted to nitrogen forms that are useable by phytoplankton. This N_2 fixation imprints a unique isotopic signature on the nitrate pool below the surface layer, which remains evident in Agulhas waters that enter the South Atlantic, potentially providing a tool to track Agulhas leakage, today and in the past.

Key Points:

- Water masses in the greater Agulhas region have distinct biogeochemical properties that reflect local and remote nitrogen cycling
- Photosynthetic nitrate assimilation dominates the mixed-layer nitrogen cycle while in situ nitrification is negligible
- Local N_2 fixation and internal nitrogen cycling imprint a signal on Indian Ocean nitrate that can be tracked into the Atlantic Ocean

Supporting Information:

Supporting Information may be found in the online version of this article.

Correspondence to:

T. A. Marshall,
mrstan001@myuct.ac.za

Citation:

Marshall, T. A., Sigman, D. M., Beal, L. M., Foreman, A., Martínez-García, A., Blain, S., et al. (2023). The Agulhas Current transports signals of local and remote Indian Ocean nitrogen cycling. *Journal of Geophysical Research: Oceans*, *128*, e2022JC019413. https://doi.org/10.1029/2022JC019413

Received 21 OCT 2022
Accepted 14 FEB 2023

Author Contributions:

Conceptualization: Tanya A. Marshall, Daniel M. Sigman, Lisa M. Beal, Alan Foreman, Alfredo Martínez-García, François Fripiat, Sarah E. Fawcett
Data curation: Alan Foreman, Alfredo Martínez-García, Stéphane Blain, Ethan Campbell, Robyn Granger, Sergey Oleynik, Raymond Roman, Kolisa Sinyanya, Sandi M. Smart, Sarah E. Fawcett
Formal analysis: Tanya A. Marshall, Daniel M. Sigman, Lisa M. Beal, Sarah E. Fawcett

1. Introduction

The role that western boundary currents (WBCs) play in Earth's climate system by transporting heat and salt from low- to higher latitudes is well-known (Bryden & Beal, 2001; Imawaki et al., 2013; Talley et al., 2011; Yu

Funding acquisition: Daniel M. Sigman, Alfredo Martínez-García, Gerald H. Haug, Sarah E. Fawcett
Investigation: Tanya A. Marshall, Daniel M. Sigman, Lisa M. Beal, Alan Foreman, Alfredo Martínez-García, Stéphane Blain, Ethan Campbell, François Fripiat, Robyn Granger, Eesaa Harris, Sergey Oleynik, Raymond Roman, Kolisa Sinyanya, Sandi M. Smart, Sarah E. Fawcett
Methodology: Tanya A. Marshall, Daniel M. Sigman, Sergey Oleynik, Sarah E. Fawcett
Project Administration: Tanya A. Marshall, Sarah E. Fawcett
Resources: Daniel M. Sigman, Lisa M. Beal, Alfredo Martínez-García, Stéphane Blain, Gerald H. Haug, Sarah E. Fawcett
Supervision: Daniel M. Sigman, Lisa M. Beal, Sarah E. Fawcett
Visualization: Tanya A. Marshall, Daniel M. Sigman, Lisa M. Beal, Patrick A. Rafter, Sarah E. Fawcett
Writing – original draft: Tanya A. Marshall, Lisa M. Beal, Sarah E. Fawcett
Writing – review & editing: Tanya A. Marshall, Daniel M. Sigman, Lisa M. Beal, Alan Foreman, Stéphane Blain, Ethan Campbell, François Fripiat, Robyn Granger, Eesaa Harris, Gerald H. Haug, Dario Marconi, Sergey Oleynik, Patrick A. Rafter, Raymond Roman, Kolisa Sinyanya, Sandi M. Smart, Sarah E. Fawcett

& Weller, 2007). The resultant net heat loss observed across WBCs strengthens the solubility pump leading to enhanced dissolution of atmospheric CO_2 in surface waters (Cronin et al., 2010; Imawaki et al., 2013; Takahashi et al., 2009; Yu & Weller, 2007). WBCs also transport nutrients from the low-latitude tropics to the subtropical and subpolar gyres in subsurface "nutrient streams" (Pelegrí & Csanady, 1991). The eventual induction of these nutrients into the mixed layer of the gyres fuels biological production (Guo et al., 2012; Pelegrí & Csanady, 1991; Williams et al., 2006). While recent measurements have quantified heat and salt properties and fluxes in and near the Agulhas Current, which is the WBC of the South Indian Ocean (Gunn et al., 2020; McMonigal et al., 2020), the sources and cycling of nutrients in Agulhas waters have yet to be investigated.

The Agulhas Current flows south-west along the steep southern African continental slope between 27°S and 37°S (Figure 1). Its transport volume is approximately 77 ± 5 Sv ($1\ \text{Sv} = 1 \times 10^6\ \text{m}^3.\text{s}^{-1}$) (Beal et al., 2015), which makes it the strongest boundary current for its latitude (Bryden et al., 2005). The Agulhas Current derives its waters from three source regions; the Mozambique Channel, the South East Madagascar Current, and recirculating subtropical gyre waters (Beal et al., 2006; Donohue & Toole, 2003; Stramma & Lutjeharms, 1997). Toward the southern tip of Africa, the Agulhas Current makes an abrupt anticlockwise retroflection to flow eastward toward the Indian Ocean as the Agulhas Return Current (Bang, 1970; Gordon, 2003; Lutjeharms, 1980). By 70°E, the majority of the waters in the Agulhas Return Current have recirculated into the subtropical southwest Indian Ocean, implying that the Return Current contributes significantly to the recirculation that ultimately supplies the Agulhas Current (Grand, Measures, Hatta, Morton, et al., 2015; Lutjeharms & Ansorge, 2001; Stramma & Lutjeharms, 1997). At the Agulhas Retroflection, 9 ± 4 Sv of Indian Ocean waters "leak" into the South Atlantic each year (de Ruijter et al., 1999; Richardson, 2007; Souza et al., 2011). This Agulhas leakage plays a role in maintaining the Atlantic Meridional Overturning Circulation (AMOC) through the addition of heat and salt to the Atlantic Ocean (Beal et al., 2011; Gordon, 1985).

WBC systems (i.e., the WBC and adjacent subtropical gyre waters) are regions of high eddy kinetic energy (Bryden et al., 2005; Ducet et al., 2000; Imawaki et al., 2013; Krug et al., 2017; Lévy et al., 2012; Schubert et al., 2019; Thomas et al., 2013) and their eddies are often associated with increased mixing. However, the strong cross-stream potential vorticity gradient and kinematic steering typical of WBCs tend to inhibit lateral mixing across the current core (Beal et al., 2006; Bower et al., 1985; Howe et al., 2009). In the Agulhas Current, a consequence of this inhibited lateral mixing is a clear, physical partitioning of tropical waters from subtropical waters at the dynamical front (Beal et al., 2006). Along the inshore side of the Agulhas Current, tropical waters are warmer, fresher, and older than subtropical waters, which are cooler, more saline, and younger (Figures 2a and 2b) (Beal et al., 2006; Gordon, 1987). Mixing can and does occur elsewhere in the current, such as across the current edges, within the mixed layer, and in the deep waters below the potential vorticity gradient and kinematic steering level near 2,000 m (Beal et al., 2006; Bower, 1991; Leber & Beal, 2015; Palter et al., 2013). How the dynamical front in the Agulhas Current impacts the distribution of nutrients is yet to be explored.

The surface waters of WBC systems are typically nitrogen (N) limited (S. Smith, 1984; Voss et al., 2013). The availability of this nutrient thus exerts a dominant control on primary productivity and carbon export. In subtropical gyres, winter convective mixing supplies subsurface nitrate (NO_3^-) to the euphotic zone, with strong stratification during the remainder of the year impeding the upward mixing of nitrate (Lomas et al., 2013; Palter et al., 2005; Williams & Follows, 2003; Williams et al., 2006). Nitrogen can also be supplied via N_2 fixation, a process mediated by diazotrophs (i.e., specialized plankton capable of transforming atmospheric N_2 gas into bioavailable or "fixed" N) that typically occurs in the warm, sunlit surface layer (Landolfi et al., 2018). Incidences of N_2 fixation have been diagnosed in subtropical waters adjacent to and within WBCs (Armbrecht et al., 2015; Detoni et al., 2016; Palter et al., 2020; Shiozaki et al., 2015; Wen et al., 2022; Wu et al., 2018), although the Agulhas Current remains unstudied in this regard.

Both newly fixed N and nitrate supplied from depth are considered "new" N sources to the mixed layer, fueling phytoplankton growth termed "new production" (Dugdale & Goering, 1967). On an annual timescale, new production must be balanced by the export of organic matter from the surface layer (i.e., "export production"), and can thus be used to infer carbon export potential (Eppley & Peterson, 1979). This mass balance approach for estimating export production is complicated if nitrification, the microbial oxidation of ammonium to nitrite and then nitrate, occurs in the euphotic zone coincident with nitrate assimilation. If so, it yields regenerated (rather than new) nitrate, the assimilation of which supports "regenerated production" (Dugdale & Goering, 1967). Failing to account for surface-layer nitrification, if significant relative to the upward supply of subsurface nitrate, will cause carbon export potential to be overestimated (Mdutyana et al., 2020; Yool et al., 2007).

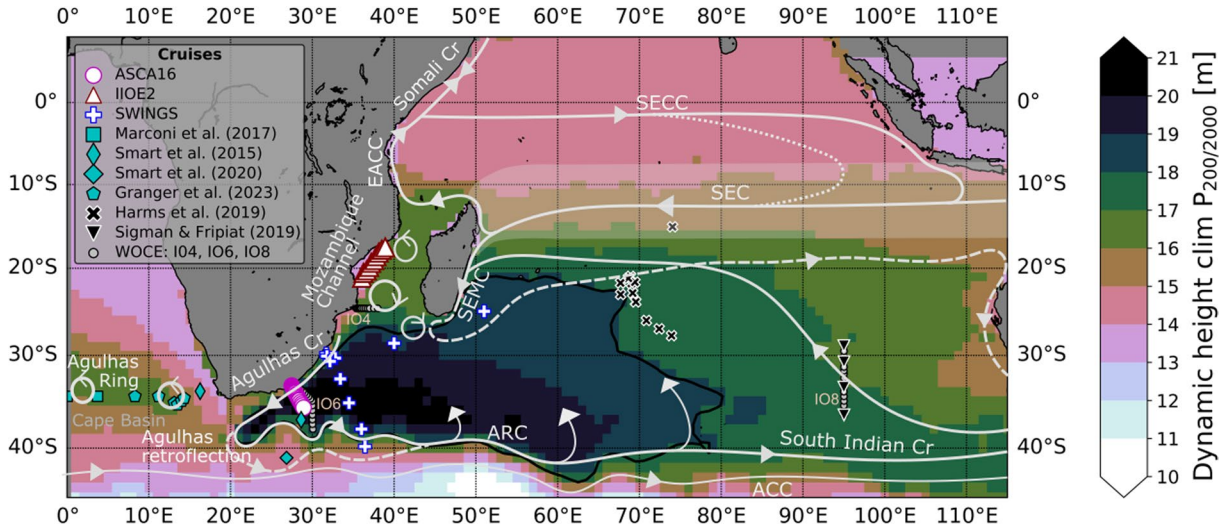

Figure 1. Thermocline circulation in the South Indian Ocean. Map showing the station locations (symbols) and thermocline circulation of the South Indian Ocean overlaid on an annual climatology of mean dynamic height for $P_{200/2000}$, which represents the mean circulation at 200 dbar referenced to 2,000 dbar. Open pink circles show stations sampled during the ASCA16 cruise, open maroon triangles indicate stations sampled during the IIOE2 cruise, and open blue pluses show stations sampled during the SWINGS cruise. Cyan symbols show the locations of earlier studies that measured nitrate isotopes in Agulhas features (R. Granger et al., 2023; Marconi et al., 2017; Smart et al., 2015, 2020), while black symbols indicate the locations of published nitrate isotope data from the South Indian Ocean (Harms et al., 2019; Sigman & Fripiat, 2019). Small white circles show the three WOCE lines; IO4 along 24°S, IO6 along ~30°E, and IO8 along 95°E. The white arrows represent the approximate thermocline circulation and circles with arrows indicate eddies. The black line shows the 18 m dynamic height contour that encompasses the region of retentive subtropical recirculation, and the dashed arrows represent the surface and seasonal currents. SEC, South Equatorial Current (the opaque shading around the SEC represents its broad meridional extent; (Talley et al., 2011)); SECC, South Equatorial Countercurrent; EACC, East African Coastal Current; SEMC, South East Madagascar Current; ARC, Agulhas Return Current; ACC, Antarctic Circumpolar Current. To derive the mean dynamic height climatology for 2004–2018, we used data from the updated Roemmich-Gilson Argo Climatology (Roemmich & Gilson, 2009). These data were collected and made freely available by the International Argo Program and the national programs that contribute to it (https://argo.ucsd.edu, https://www.ocean-ops.org). The Argo Program is part of the Global Ocean Observing System (Argo, 2021).

In the Indian Ocean, model-based mean estimates of N_2 fixation and denitrification (i.e., the removal of fixed N) are approximately 26 and 40 Tg N.a^{-1}, respectively (Bianchi et al., 2012; Deutsch et al., 2007; DeVries et al., 2013; Landolfi et al., 2018; Wang et al., 2019). The imbalance between these two fluxes implies that N loss is not completely offset by N gain in the Indian Ocean. N_2 fixation measured in the euphotic zone of the Arabian Sea, a region that supports high rates of denitrification, contributes only ~10% of the basin-wide N gain (2.3 Tg N.a^{-1}; (Bange et al., 2000; Capone et al., 1998; Gandhi et al., 2011)). Therefore, N_2 fixation must be significant elsewhere in the Indian Ocean (Deutsch et al., 2007; Grand, Measures, Hatta, Morton, et al., 2015; Gruber & Sarmiento, 1997; Wang et al., 2019), yet there are almost no observations of this process, particularly from the southern basin (cf. Harms et al., 2019; Karlusich et al., 2021; Metzl et al., 2022; Poulton et al., 2009).

Here, we use measurements of hydrography, nutrients, and the N and oxygen (O) isotopes of nitrate across the southwest Indian Ocean to investigate circulation and N cycling. Our goals are to (a) biogeochemically characterize the regional water masses to better understand their sources and circulation and (b) diagnose regional N cycle processes such as N_2 fixation, nitrate assimilation, and nitrification. The nitrate isotopes are well suited for investigating circulation and N cycling for three main reasons. First, nitrate isotope ratios in the waters beneath the thermocline record preformed signals that can be used to trace water masses and their subsequent modification between formation and our study site (e.g., (Marconi et al., 2017; Rafter et al., 2013)). Second, any (de)coupling of the N and O isotope ratios in the thermocline and mixed layer allows us to disentangle nitrate assimilation from nitrification and thus to evaluate the relative importance of nitrate supplied to the mixed layer from the subsurface (which fuels new production) versus nitrate regenerated within the mixed layer (which fuels regenerated production). Third, the nitrate isotopes record and integrate the signal of N_2 fixation and as such, can be used to evaluate the proportion of locally produced versus transported newly fixed nitrate in the southwest Indian Ocean (Knapp et al., 2005, 2008; Marconi et al., 2017; Marshall et al., 2022).

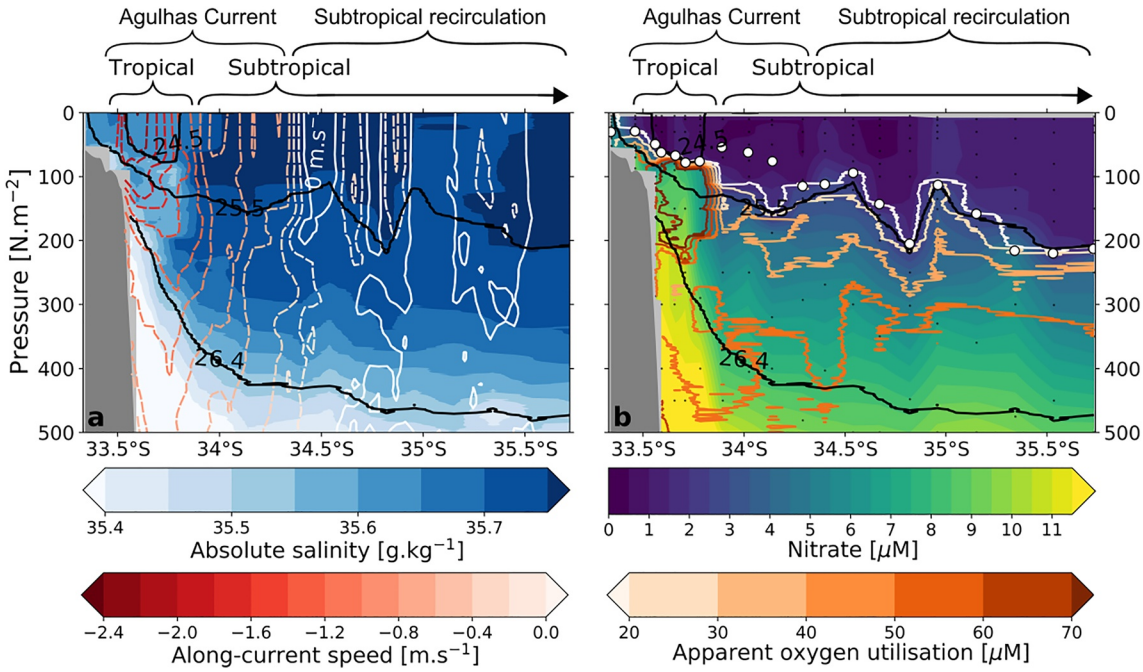

Figure 2. Structure of the Agulhas Current and recirculating waters. (a) Gridded depth section of absolute salinity [g.kg^{-1}] over the upper 500 m of the ASCA16 transect. Overlaid in shades of red are contours of along-current speed [m.s^{-1}] measured from a shipboard acoustic Doppler current profiler. (b) Gridded depth section of nitrate concentration [μM] over the upper 500 m of the ASCA16 transect. Overlaid in shades of orange are contours of apparent oxygen utilization (AOU) [μM]. Small white circles indicate the mixed layer depth at each station. In both (a and b), black contours show the isopycnal boundaries of the major water masses (see Table 1). The top row of brackets indicates the position of the fast-flowing Agulhas Current and adjacent subtropical recirculation. The bottom row of brackets distinguishes the fresh, high-AOU, high-nitrate, tropically sourced waters along the inshore side of the Agulhas Current from the saline, lower-AOU, lower-nitrate, subtropically sourced waters along the offshore side of the Agulhas Current. The shoaling isopycnals that uplift nutrient-rich waters within the Agulhas Current are consistent with observations of subsurface nutrient streams reported in other WBCs (Pelegrí & Csanady, 1991).

2. Methods

2.1. Field Sampling

During three cruises to the southwest Indian Ocean, we collected full-depth hydrographic data and seawater samples for nutrient and nitrate isotope analysis. Twenty stations were occupied across the Agulhas Current and adjacent recirculating waters along the Agulhas System Climate Array near ~34°S in austral winter, July 2016 (ASCA16), onboard the R/V *SA Agulhas II* (circles outlined in pink in Figure 1). Ten stations were occupied along the western slope of the Mozambique Channel along ~37°E (which sampled to ~1,500 m) in austral spring, October 2017, as part of a larger study of the African continental shelf (IIOE2; iioe-2.incois.gov.in), also onboard the R/V *SA Agulhas II* (triangles outlined in red in Figure 1). Finally, 10 stations were occupied across the southwest Indian Ocean, with four stations in the Agulhas Current (near ~30°S) and six in the subtropical recirculation, in austral summer, January 2021, as part of the GEOTRACES SWINGS cruise (swings.geotraces.org) onboard the R/V *Marion-Dufresne* (pluses outlined in blue in Figure 1).

All hydrographic measurements were made using a Conductivity-Temperature-Depth-Oxygen (CTDO) sensor attached to a Seabird 9/11+ rosette equipped with 12 L Niskin bottles. Potential density anomalies referenced to 0 dbar (σ_0), 2,000 dbar (σ_2), and 4,000 dbar (σ_4) pressure levels were derived from conservative temperature and absolute salinity using the Gibbs Seawater Oceanographic package in Python. Apparent oxygen utilization (AOU) was calculated as the difference between the derived oxygen saturation concentration at a given salinity and temperature and the observed oxygen concentration (i.e., AOU, in μM, = $[O_{2saturated}]$–$[O_{2observed}]$). Duplicate seawater samples were collected throughout the water column for nutrients and nitrate isotopes in thoroughly rinsed 50 ml Falcon tubes and high-density polyethylene bottles, respectively. All nitrate isotope samples and the nutrient samples from ASCA16 and IIOE2 were frozen at −20°C directly after collection while the SWINGS nutrient samples were syringe-filtered (0.45 μm) shipboard, then poisoned with mercuric chloride (20 mg.L^{-1} final concentration) and stored at room temperature until analysis.

During the ASCA16 cruise, a ship-mounted 75 kHz Teledyne RD acoustic Doppler current profiler collected velocity data from 45 to ~850 m. These data were rotated normal to the Agulhas Current and extended from 45 m to the surface.

2.2. Nutrient Analyses

Samples were measured for nitrate, silicic acid ($Si(OH)_4$), and nitrite (NO_2^-) concentrations in the Marine Biogeochemistry Lab at the University of Cape Town (UCT-MBL; for ASCA16 and IIOE2) and in the Microbial Oceanography Laboratory at the Sorbonne Université (for SWINGS). Full-depth distributions of nitrate, nitrite, and silicic acid concentrations for ASCA16 are shown in Supporting Information S1 (Figure S1), for SWINGS in Supporting Information S1 (Figure S2), and for IIOE2 in Supporting Information S1 (Figure S3). In the UCT-MBL, nitrate + nitrite and silicic acid concentrations were measured using a Lachat QuickChem® Flow Injection Analysis platform (Diamond, 1994; Grasshoff, 1976) with a precision of 0.2 μM and detection limit of 0.1 μM. Nitrite concentrations were measured manually using standard colorimetric methods (Grasshoff, 1976; Strickland & Parsons, 1972) and a Genesys 30 Visible spectrophotometer, with a precision of 0.1 μM and a detection limit of 0.05 μM. In the Microbial Oceanography Laboratory, nitrate + nitrite, nitrite, and silicic acid concentrations were determined using a Skalar segmented flow analyzer (Blain et al., 2015) with a precision of 1%–4% and detection limits of 0.02 μM for nitrate + nitrite and nitrite and 0.1 μM for silicic acid. Certified reference materials (JAMSTEC for ASCA16 and IIOE2 and Certipur for SWINGS) were included in all runs to ensure measurement accuracy. Nitrate concentrations were calculated as the difference between the nitrate + nitrite and nitrite concentrations. Hereafter, all references to nitrate concentration are to the nitrate-only data.

2.3. Nitrate N and O Isotope Analyses

All nitrate isotope samples were syringe-filtered (0.2 μm) to remove organic matter. Prior to isotopic analysis, samples with nitrite concentrations >0.5% of the nitrate + nitrite concentrations were treated with sulfamic acid to remove nitrite, followed by 2 M sodium hydroxide to return the sample pH to between 7 and 8 (J. Granger & Sigman, 2009). The removal of nitrite is necessary because its isotopic composition can differ greatly from that of nitrate, such that even when present at low concentrations, nitrite can have a significant effect on the $\delta^{15}N$ and $\delta^{18}O$ of the nitrate + nitrite pool (Casciotti & McIlvin, 2007; Fawcett et al., 2015; J. Granger & Sigman, 2009; Kemeny et al., 2016).

The natural abundance N and O isotope ratios of nitrate are reported in delta (δ) notation as $\delta^{15}N$, in ‰ versus N_2 in air, $= [(^{15}N/^{14}N)_{sample}/(^{15}N/^{14}N)_{reference} - 1] \times 10^3$ and $\delta^{18}O$, in ‰ versus VSMOW, $= [(^{18}O/^{16}O)_{sample}/(^{18}O/^{16}O)_{reference} - 1] \times 10^3$. The nitrate isotopes were measured at Princeton University (ASCA16; $\delta^{15}N$ and $\delta^{18}O$) and the Max Planck Institute for Chemistry (IIOE2 and SWINGS, with only $\delta^{15}N$ data available for SWINGS) using the "denitrifier" method (Casciotti et al., 2002; Sigman et al., 2001). This method relies on the bacterial reduction of nitrate to nitrous oxide gas (N_2O), after which a Thermo MAT 253 isotope ratio mass spectrometer interfaced with a custom-built online N_2O extraction and purification system was used to measure the N and O isotopic composition of the N_2O (Casciotti et al., 2002; Sigman et al., 2001; Weigand et al., 2016). International reference materials, IAEA-N3 and USGS-34 (Böhlke et al., 2003; Gonfiantini, 1984), as well as an in-house N_2O standard, were run in parallel with the samples. The pooled standard deviation of replicate measurements of nitrate $\delta^{15}N$ and $\delta^{18}O$ for the ASCA16 samples was 0.10 and 0.20‰ ($n = 281$; all samples with nitrate concentrations >0.35 μM were measured), for the IIOE2 samples was 0.12 and 0.15‰ ($n = 103$, all samples with nitrate concentrations >1.76 μM were measured), and for the SWINGS samples was 0.17‰ ($\delta^{15}N$ only, $n = 172$, all samples with nitrate concentrations >0.96 μM were measured). The nitrate $\delta^{18}O$ data were not corrected for depth-related changes in salinity (Knapp et al., 2008) as the vertical salinity gradients were relatively minor and there is considerable uncertainty associated with the $\delta^{18}O_{H2O}$/salinity relationship in the subtropical Indian Ocean (Schmidt et al., 1999; Text S1 in Supporting Information S1).

2.3.1. The Dual Isotopes of Nitrate

Nitrate $\delta^{15}N$ and $\delta^{18}O$ can separately yield insights into oceanic N cycling; however, their dual measurement increases their utility, allowing overlapping processes to be disentangled (e.g., Fawcett et al., 2015; Rafter et al., 2013; Sigman et al., 2005). During nitrate assimilation, phytoplankton preferentially consume the lighter ^{14}N and ^{16}O isotopes, causing the $\delta^{15}N$ and $\delta^{18}O$ of the ambient nitrate pool to increase as its concentration declines

(Casciotti et al., 2002; Sigman et al., 1999; Wada & Hattori, 1976). This increase occurs in a ratio of ~1:1 (i.e., the rise in nitrate $\delta^{15}N$ is coupled to that of $\delta^{18}O$; (J. Granger et al., 2004, 2010)). Denitrification also raises the $\delta^{15}N$ and $\delta^{18}O$ of nitrate in tandem (J. Granger et al., 2008). By contrast, during nitrification, the $\delta^{15}N$ and $\delta^{18}O$ of nitrate are decoupled because the $\delta^{15}N$ of newly nitrified nitrate is set by the $\delta^{15}N$ of the organic matter plus ammonium being remineralized and oxidized while its $\delta^{18}O$ is strongly controlled by the $\delta^{18}O$ of seawater (i.e., the $\delta^{18}O$ of newly nitrified nitrate has been shown to equal $\delta^{18}O_{H2O}$, = ~0‰, plus an isotopic offset of ~1.1‰; (Boshers et al., 2019; Buchwald et al., 2012; Marconi et al., 2019; Sigman et al., 2009)).

The parameter nitrate $\Delta(15–18)$ ($= \delta^{15}N - \delta^{18}O$) leverages the (de)coupling of nitrate $\delta^{15}N$ and $\delta^{18}O$ and as such, is useful for identifying overlapping N cycle processes (Rafter et al., 2013; Sigman et al., 2005). In surface waters where photosynthetic nitrate assimilation is dominant, we expect nitrate $\Delta(15–18)$ to remain constant (e.g., (DiFiore et al., 2009; Fawcett et al., 2015)) as nitrate $\delta^{15}N$ and $\delta^{18}O$ rise in unison (J. Granger et al., 2004, 2010). In the underlying thermocline where organic matter deriving from surface productivity is remineralized, nitrate $\Delta(15–18)$ may increase or decrease depending on the $\delta^{15}N$ of the remineralized organic matter relative to the $\delta^{18}O$ of newly nitrified nitrate. Since N_2 fixation introduces organic matter with a $\delta^{15}N$ of approximately −1‰ (Carpenter et al., 1997; Hoering & Ford, 1960; Minagawa & Wada, 1986), which is low relative to subsurface nitrate (which ranges in $\delta^{15}N$ from roughly 3–7‰ (Fripiat et al., 2021; Knapp et al., 2008; Rafter et al., 2013, 2019; Sigman et al., 1999)), its remineralization yields nitrate with a low $\delta^{15}N$ and $\Delta(15–18)$ (Knapp et al., 2005, 2008; Lehmann et al., 2018; Rafter et al., 2013; Sigman et al., 2005, 2009). Co-occurring partial nitrate assimilation and nitrification also yields low-$\Delta(15–18)$ nitrate (Deman et al., 2021; Fawcett et al., 2015; Rafter et al., 2013; Sigman et al., 2005, 2009). This is because the cycling of N between nitrate assimilation and nitrification has little effect on the $\delta^{15}N$ of nitrate as in net, N is neither lost nor gained. Contrastingly, nitrate assimilation is a sink for the O atoms of nitrate and nitrification is the ultimate source, such that the $\delta^{18}O$ of nitrate is "reset" by nitrification. In the case of co-occurring partial nitrate assimilation and nitrification, the $\delta^{18}O$ of the combined partially assimilated and newly nitrified nitrate pool ends up higher than the $\delta^{18}O$ of the nitrate initially removed by phytoplankton (Fawcett et al., 2015; Rafter et al., 2013; Sigman et al., 2005, 2009).

3. Results and Interpretation

We report our findings in the context of the regional water masses, presenting their biogeochemical properties for the first time. Mean values of measured hydrographic and biogeochemical properties for the Agulhas Current and adjacent recirculating waters are included in Table 1 (ASCA16 plus SWINGS) and for the western Mozambique Channel (IIOE2), in Table 2. The divide created by the dynamical front in the Agulhas Current is most apparent in the upper ocean ($\sigma_\theta < 26.4$ kg.m^{-3}) water mass properties (Figure 3). Subtropical waters are present at ASCA16 stations south of 33.78°S and at SWINGS stations east of ~33°E (circles and pluses in Figure 3; blue circles and green pentagons in Figure 4), while tropical waters occur at ASCA16 stations north of and including 33.78°S and at SWINGS stations west of and including 33°E (stars and diamonds in Figure 3; pink circles and purple pentagons in Figure 4). We treat the subtropical waters in the Agulhas Current and the adjacent recirculating waters from the subtropical gyre collectively (Table 1) since the Agulhas Current sources the majority of its water from the recirculation. Because ASCA16 was sampled at higher resolution and the data set includes nitrate $\delta^{18}O$ (and therefore $\Delta(15–18)$), we focus our analysis on the nitrate dual isotope data from the ASCA16 cruise, incorporating the nitrate concentration and $\delta^{15}N$ data from the SWINGS cruise only where relevant.

3.1. Source Waters of the Southwest Indian Ocean

Our biogeochemical measurements yield new insights into the origins and modifications of water masses in the southwest Indian Ocean. The Agulhas Current water masses were first defined by Beal et al. (2006) based on salinity, potential vorticity, and oxygen concentrations. By also considering the biogeochemistry, we can refine the original water masses definitions and identify additional water masses from their distinctive biogeochemical properties (Figures 3 and 4). For example, we distinguish between thermocline and sub-thermocline waters, which are often collectively described as "central waters" (~25.0 kg.m^{-3} < σ_θ < 27.0 kg.m^{-3}). Thermocline waters ($\sigma_\theta < 26.4$ kg.m^{-3}) are influenced by the remineralization of organic matter produced in the overlying surface waters as well as by the upward supply of nutrients from below (e.g., during deep winter/spring mixing), while sub-thermocline waters ($\sigma_\theta > 26.4$ kg.m^{-3}) constitute the ultimate source of nutrients to the overlying thermocline and surface layer. Additionally, we use knowledge of water mass biogeochemistry at the sites of

Journal of Geophysical Research: Oceans

10.1029/2022JC019413

Table 1
Water Mass Characteristics in the Subtropical Southwest Indian Ocean

Water mass		Abbreviation	Potential density, σ_θ [kg.m^{-3}]	Absolute salinity [g.kg^{-1}]	Conservative temperature, θ [°C]	Oxygen [μM]	AOU [μM]	NO_3^- [μM]	$\delta^{15}N$ NO_3^- [‰]	$\delta^{18}O$ NO_3^- [‰][a]	Δ(15–18) [‰][a]
Tropical	Tropical Surface Water	TSW	<24.5	35.6 ± 0.51	22.8 ± 1.37	200.8 ± 9.3	12.9 ± 4.8	1.1 ± 0.9 (0.2 ± 0.1)	6.5 ± 1.2 (NA)	4.0 ± 1.2	2.5 ± 1.2
	Tropical Thermocline Water	TTW	24.5–26.4	35.6 ± 0.05	17.4 ± 2.26	179.8 ± 27.7	73.4 ± 13.6	7.8 ± 1.8 (9.6 ± 2.5)	5.8 ± 0.3 (6.2 ± 0.4)	2.7 ± 0.4	3.2 ± 0.3
Subtropical	Subtropical Surface Water	STSW	<25.5	35.7 ± 0.11	20.1 ± 1.47	212.2 ± 14.1	10.2 ± 7.6	1.0 ± 0.5 (0.4 ± 0.6)	8.0 ± 0.7 (6.0 ± 1.9)	6.7 ± 0.7	1.3 ± 0.8
	Subtropical Thermocline Water	STTW	25.5–26.4	35.7 ± 0.03	18.3 ± 0.99	199.4 ± 16.5	28.3 ± 11.3	3.0 ± 1.4 (3.0 ± 1.4)	4.9 ± 0.7 (5.1 ± 0.7)	2.8 ± 0.8	2.1 ± 0.8
Subantarctic Mode Water		SAMW	26.4–27.0	35.1 ± 0.23 [35.1 ± 0.05]	11.0 ± 1.86 [11.3 ± 0.38]	203.6 ± 8.6 [209.4 ± 4.7]	65.4 ± 16.3 [57.4 ± 4.4]	15.2 ± 4.3 (15.3 ± 3.9) [13.8 ± 1.1]	6.7 ± 0.4 (6.6 ± 0.5) [6.9 ± 0.1]	3.3 ± 0.4 [3.5 ± 0.1]	3.4 ± 0.4 [3.4 ± 0.1]
Antarctic Intermediate Water		AAIW	27.0–27.4	34.6 ± 0.06	5.4 ± 1.06	177.8 ± 14.9	128.4 ± 18.0	28.3 ± 2.4 (31.6 ± 2.4)	6.0 ± 0.1 (6.0 ± 0.1)	2.6 ± 0.1	3.4 ± 0.1
Red Sea Water lenses		RSW	27.45–27.55	34.8 ± 0.04	4.1 ± 0.28	150.3 ± 8.8	166.8 ± 7.0	31.9 ± 0.7 (31.5 ± 2.0)	6.0 ± 0.0 (5.9 ± 0.1)	2.6 ± 0.1	3.4 ± 0.0
Upper Circumpolar Deep Water		UCDW	27.4 to $\sigma_2 = 36.9$	34.8 ± 0.07	3.1 ± 0.46	164.3 ± 10.5	160.1 ± 7.6	30.7 ± 1.3 (31.7 ± 2.0)	5.5 ± 0.1 (5.5 ± 0.1)	2.2 ± 0.1	3.4 ± 0.1
Indian Deep Water		IDW	27.45 to $\sigma_4 = 45.9$	(34.9 ± 0.00)	(1.8 ± 0.04)	(211.9 ± 0.3)	(177.3 ± 0.4)	(35 ± 0.1)	(5.4 ± 0.0)	–	–
North Atlantic Deep Water		NADW	$\sigma_2 = 36.9$ to $\sigma_4 = 45.9$	35.0 ± 0.02	2.1 ± 0.31	202.2 ± 8.4	129.1 ± 6.7	27.4 ± 0.8 (29.1 ± 1.4)	5.0 ± 0.00 (5.1 ± 0.1)	1.9 ± 0.1	3.1 ± 0.1
Lower Circumpolar Deep Water		LCDW	$\sigma_4 > 45.9$	34.9 ± 0.02	0.9 ± 0.32	208.2 ± 2.5	134.7 ± 2.8	29.3 ± 0.8 (30.9 ± 1.0)	4.9 ± 0.0 (4.9 ± 0.0)	1.8 ± 0.1	3.0 ± 0.0

Note. Mean values (±1 SD) of absolute salinity [g.kg^{-1}], conservative temperature, θ [°C], oxygen concentration [μM], apparent oxygen utilization (AOU) [μM], nitrate concentration [μM], and concentration-weighted nitrate $\delta^{15}N$ [‰], $\delta^{18}O$ [‰], and Δ(15–18) [‰] for the water masses identified in the ASCA16 and SWINGS data sets. Nitrate $\delta^{18}O$ and Δ(15–18) are included for the ASCA16 data set only. For the other parameters, values from the SWINGS data set are provided in soft brackets. Water masses are defined by potential density anomalies, σ_θ [kg.m^{-3}], with the core properties of Subantarctic Mode Water, the ultimate source water to the region, listed in square brackets. The narrow density range occupied by the surface and thermocline waters condenses the data in density space (Text S3 in Supporting Information S1); we thus report surface and thermocline water mass properties averaged over depth rather than density (the density-defined values are provided separately in Tables S1 in Supporting Information S1 (for ASCA16) and S2 (for SWINGS)). The row subheadings *Tropical* and *Subtropical* refer to the waters inshore and offshore of the Agulhas Current core, respectively. Tropical (subtropical) waters occur at ASCA16 stations north (south) of 33.78°S and at SWINGS stations west (east) of ~33°E. The two most coastal ASCA16 stations (33.34°S and 33.46°S) are excluded from the inshore means as both are influenced by shelf upwelling, which is evident in their elevated density, nitrate concentration, and nitrate-Δ(15–18) values that resemble deeper waters. The Abbreviation column lists the abbreviations for the various water masses used throughout this study.

[a]Data from ASCA16 only.

Journal of Geophysical Research: Oceans

10.1029/2022JC019413

Table 2
Water Mass Characteristics in the Western Mozambique Channel

Water mass	Abbreviation	Potential density, σ_θ [kg.m^{-3}]	Absolute salinity [g.kg^{-1}]	Conservative temperature, θ [°C]	Oxygen [μM]	AOU [μM]	NO_3^- [μM]	$\delta^{15}N$ NO_3^- [‰]	$\delta^{18}O$ NO_3^- [‰]	Δ(15–18) [‰]
Tropical Surface Water	TSW	<24.5	35.4 ± 0.05	25.0 ± 1.36	180.2 ± 14.5	25.9 ± 19.0	2.2 ± 2.0	6.5 ± 1.3	3.0 ± 1.3	3.6 ± 1.3
Tropical Thermocline Water	TTW	24.5–26.4	35.5 ± 0.05	16.8 ± 2.28	139.1 ± 8.4	99.7 ± 10.1	10.9 ± 2.2	6.0 ± 0.4	2.8 ± 0.4	3.2 ± 0.4
Southeast Indian Subantarctic Mode Water	SEI-SAMW	26.4–26.9	35.1 ± 0.13 [35.1 ± 0.07]	11.2 ± 1.28 [11.2 ± 0.58]	169.0 ± 7.0 [173.2 ± 4.1]	98.9 ± 8.2 [94.3 ± 4.6]	16.9 ± 3.6 [16.4 ± 2.4]	6.7 ± 0.3 [6.8 ± 0.2]	3.2 ± 0.3 [3.3 ± 0.2]	3.5 ± 0.3 [3.5 ± 0.2]
Antarctic Intermediate Water	AAIW	26.9–27.1	34.9 ± 0.02	8.5 ± 0.44	146.1 ± 10.9	138.6 ± 13.4	24.6 ± 2.7	6.6 ± 0.1	3.0 ± 0.1	3.6 ± 0.1
Red Sea Water	RSW	27.1 to $\sigma_2 = 36.6$	35.0 ± 0.03	6.2 ± 0.83	95.6 ± 11.9	204.3 ± 15.9	32.9 ± 2.8	6.6 ± 0.1	2.9 ± 0.1	3.7 ± 0.1
Upper Circumpolar Deep Water	UCDW	$\sigma_2 > 36.6$	34.9 ± 0.03	4.0 ± 0.37	115.5 ± 10.7	200.0 ± 8.1	34.6 ± 1.3	6.1 ± 0.1	2.5 ± 0.1	3.5 ± 0.1

Note. Mean values (±1 SD) of absolute salinity [g.kg^{-1}], conservative temperature [°C], oxygen concentration [uM], apparent oxygen utilization (AOU) [μM], nitrate concentration [μM], and concentration-weighted nitrate $\delta^{15}N$ [‰], $\delta^{18}O$ [‰], and Δ(15–18) [‰] for the water masses identified in the IIOE2 data set. Water masses are defined by potential density anomalies, σ_θ [kg.m^{-3}], and the core properties of Subantarctic Mode Water are listed in square brackets.

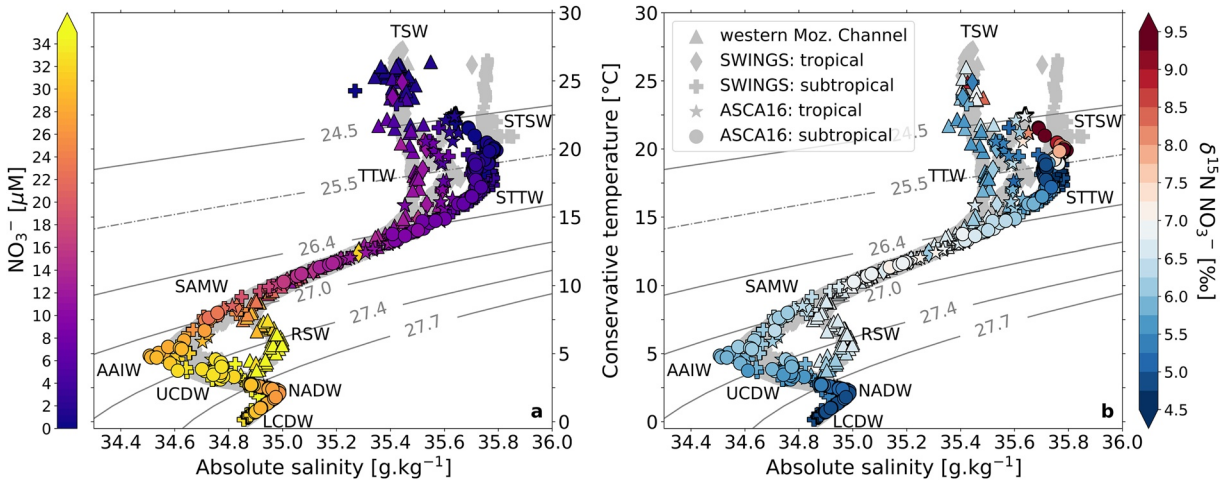

Figure 3. Biogeochemical characteristics of water masses in the southwest Indian Ocean. Conservative temperature [°C] versus absolute salinity [g.kg^{-1}] for the ASCA16 (circle and star symbols), IIOE2 (triangle symbols), and SWINGS (plus and diamond symbols) cruises. Symbol colors indicate (a) nitrate concentration [μM] and (b) nitrate δ^{15}N [‰]. ASCA16 and SWINGS stations that sampled tropical versus subtropical waters are indicated in the legend. The colored symbols show discrete samples and the underlying gray symbols show the high resolution CTDO-derived values of temperature and salinity. Gray contours indicate the potential density anomalies (labeled on the panels, in kg.m^{-3}) that form the boundaries of water masses (see Table 1). TSW, Tropical Surface Water; STSW, Subtropical Surface Water; TTW, Tropical Thermocline Water; STTW, Subtropical Thermocline Water; SAMW, Subantarctic Mode Water; AAIW, Antarctic Intermediate Water; RSW, Red Sea Water; UCDW, Upper Circumpolar Deep Water; NADW, North Atlantic Deep Water; LCDW, Lower Circumpolar Deep Water.

formation to infer modifications, and the processes responsible therefor, along the circulation pathways to our study site (Figure 5).

3.1.1. Deep Waters

Four deep water masses occupy the southwest Indian Ocean; from deepest to shallowest these are Lower Circumpolar Deep Water (LCDW; $\sigma_4 \geq 45.9$ kg.m^{-3}), North Atlantic Deep Water (NADW; $\sigma_2 = 36.9$ kg.m^{-3} to $\sigma_4 = 45.9$ kg.m^{-3}), Indian Deep Water (IDW; $\sigma_\theta = 27.45$ kg.m^{-3} to $\sigma_4 = 45.9$ kg.m^{-3}, with its core at

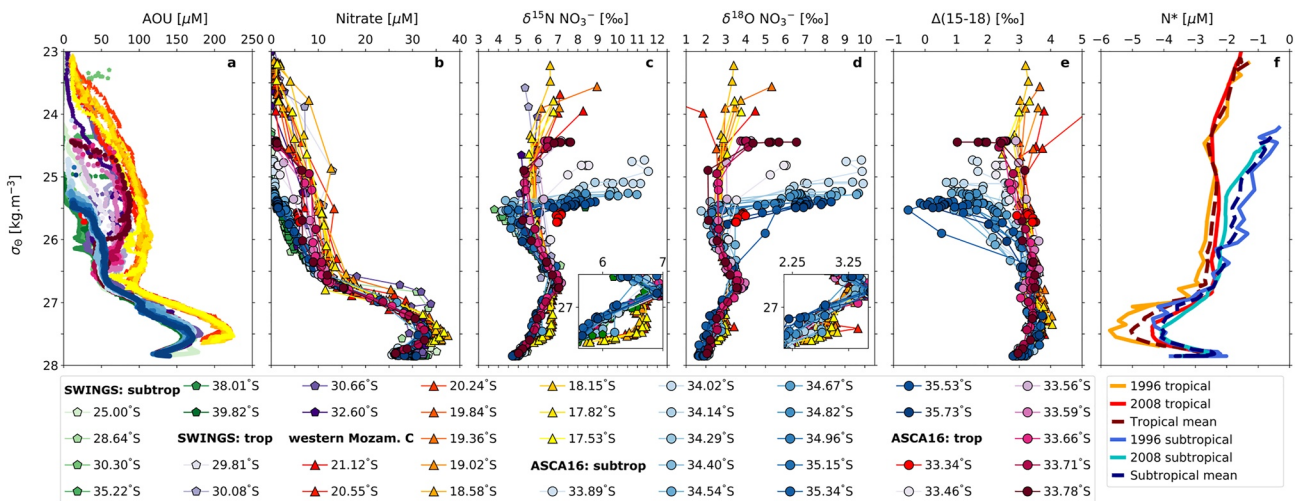

Figure 4. Biogeochemistry of the southwest Indian Ocean. Density profiles of (a) apparent oxygen utilization (AOU) [μM], (b) nitrate concentration [μM], (c) nitrate δ^{15}N [‰], (d) nitrate δ^{18}O [‰], (e) nitrate Δ(15–18) [‰], and (f) mean gridded N* [μM] (= [NO_3^-] − 16 × [PO_4^{3-}]; (Gruber & Sarmiento, 1997)). The legend provides station latitude with subheadings indicating sample region. Subtropical and tropical SWINGS data are represented by green and purple pentagons, respectively, IIEO2 data are shown by the triangle symbols and represent the western Mozambique Channel, and subtropical and tropical ASCA16 data are represented by blue and pink circles, respectively. The AOU values are derived from measurements made during CTDO deployments and as such, are available at higher vertical resolution than the discrete measurements shown in panels (b–e). The inset boxes in panels (c and d) provide a zoomed-in view of the intermediate waters. The N* data shown in panel (f) are from two occupations (1996 and 2008; solid lines) of WOCE IO6 line (near-meridional line at ~30°E). Tropical (subtropical) means for each cruise are shown in warm (cool) colors, with the inter-cruise means indicated by the dashed profiles.

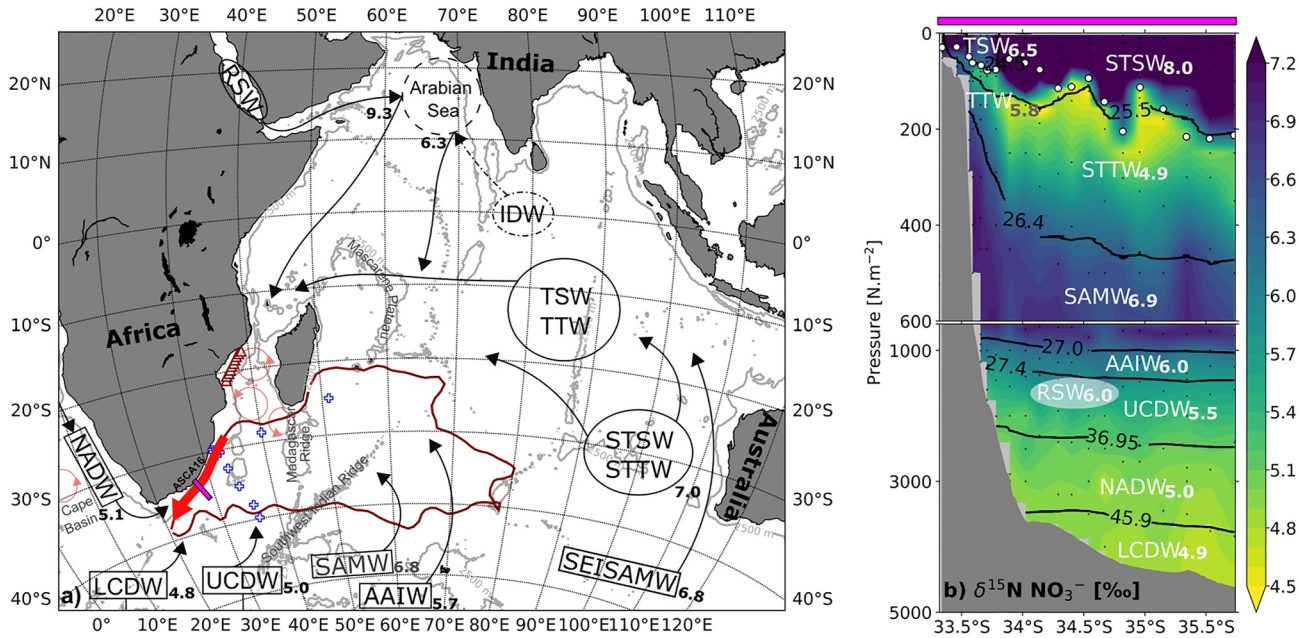

Figure 5. Source water circulation and modification in the southwest Indian Ocean. (a) Schematic of the source regions and pathways followed by the water masses that enter the southwest Indian Ocean, along with their nitrate-$\delta^{15}N$ endmembers, and (b) gridded full-depth section of nitrate $\delta^{15}N$ [‰] across the ASCA16 transect. On both panels, water mass abbreviations are as in Figure 3 and Table 1. The bold subscripted values indicate the mean nitrate $\delta^{15}N$ [‰] for each water mass, with the panel (b) values from ASCA16 (Table 1). In panel (a), water masses formed within the Indian Ocean are outlined with ovals while water masses formed outside the basin are outlined with squares. The nitrate-$\delta^{15}N$ values, where available, are those measured either at formation or prior to entering the Agulhas Current (see Section 3.1 for details). Nitrate $\delta^{15}N$ values are not provided for the (sub)tropical surface waters (i.e., $\sigma_\theta < 25.5$ kg.m^{-3}, or upper 50–100 m; Tables 1 and 2) at formation because repeated cycles of nitrate supply and assimilation in these waters alter their preformed $\delta^{15}N$. As such, the nitrate $\delta^{15}N$ subscript associated with STSW/STTW is for Subtropical Thermocline Water only. Additionally, there are no nitrate-$\delta^{15}N$ data available for Tropical Thermocline Water at formation. Indian Deep Water (IDW) has a dot-dashed line to indicate that it forms throughout the north Indian Basin and not only at the location of the circle. The gray contours represent the bathymetry at 2,500 m, with the Mascarene Plateau, Madagascar Ridge, Southwest Indian Ridge, and Cape Basin labeled in gray (data from the GEBCO Compilation Group (2022) GEBCO_2022 Grid (https://doi.org/10.5285/e0f0bb80-ab44-2739-e053-6c86abc0289c)). The thin black arrows approximate the pathways by which the water masses enter the southwest Indian Ocean. The thick red arrow indicates the Agulhas Current and the bold maroon contour encompasses the subtropical recirculation. Thin light-red circles indicate eddies in the Mozambique Channel, south of Madagascar, and in the Cape Basin. The pink line indicates the location of the ASCA16 transect, the open maroon triangles indicate the IIEO2 stations, and open blue pluses indicate the SWINGS stations. This panel is adapted from Beal et al. (2006), their Figure 5. In panel (b), black contours indicate the isopycnal boundaries of water masses (see Table 1) and small white circles show the mixed layer depth. The white opaque oval represents a Red Sea Water lens, and the black dots indicate discrete sampling depths. The *y*-axis is broken at 600 m in order to adequately resolve both the upper- and deep water masses.

σ_2 = ~37.0 kg.m^{-3}), and Upper Circumpolar Deep Water (UCDW; σ_θ = 27.4 kg.m^{-3} to σ_2 = 36.9 kg.m^{-3}) (Figures 3–5 and Tables 1 and 2). These deep water masses exchange properties via the global overturning circulation. Following the mixing of NADW with IDW (as well as Pacific Deep Water) in the ocean interior, the deep waters upwell in the Southern Ocean to form Upper and Lower CDW, eventually circulating back to the northern basins to be incorporated into newly forming deep waters (Talley, 2013; Talley et al., 2011). Here, we identify the two limbs of CDW in the Agulhas Current for the first time.

NADW is formed by deep convection in the subarctic North Atlantic where it has a mean nitrate concentration of 17.5 μM and $\delta^{15}N$ of 4.8‰ (Marconi et al., 2015; Sigman et al., 2000). Its relatively low nitrate $\delta^{15}N$ derives from N_2 fixation in the (sub)tropical North Atlantic (Deman et al., 2021; Knapp et al., 2008; Marconi et al., 2015; Marconi et al., 2017). By the time NADW reaches the southwest Indian Ocean, its mean nitrate concentration has increased to 27.4 ± 0.8 μM and its $\delta^{15}N$ to 5.0 ± 0.0‰, similar to observations from the Cape Basin (26.0 μM and 5.1‰, respectively; (Campbell, 2016; Marconi et al., 2017)). The higher nitrate concentration and $\delta^{15}N$ are likely due to NADW mixing with CDW during its southward transit toward the Southern Ocean.

IDW forms in the Indian basin through diapycnal diffusion and subsurface upwelling of NADW, Upper and Lower CDW, and deep North Indian basin waters (Donohue & Toole, 2003; Talley, 2013; Talley et al., 2011). Deep waters from the North Indian basin carry a strong remineralization and denitrification signal that is reflected in their high AOU (>230 μM) and elevated nitrate $\delta^{15}N$ (mean of 6.3 ± 0.2‰) (Harms et al., 2019; Martin &

Casciotti, 2017). We observe IDW to the east of Madagascar in one profile from the SWINGS cruise (at 25°S) where AOU reaches 177.3 ± 0.4 μM and nitrate $\delta^{15}N$ is 5.4 ± 0.0‰. The eroded properties likely result from mixing with younger deep waters that have a lower nitrate $\delta^{15}N$ (Harms et al., 2019). IDW is not found in the Agulhas Current and adjacent recirculating waters because the Mozambique and Madagascar Ridges block the south-westward flow of deep waters from the basin interior (Figure 5a).

Where LCDW upwells, typically at >60°S, it has a relatively low nitrate $\delta^{15}N$ of 4.8‰ and $\delta^{18}O$ of 1.8‰, reflecting a large contribution of low-$\delta^{15}N$ NADW nitrate (Fripiat et al., 2019; Sigman, et al., 1999; Smart et al., 2015). In the Agulhas Current region, LCDW nitrate is similarly characterized by a $\delta^{15}N$ of 4.9 ± 0.0‰ and $\delta^{18}O$ of 1.8 ± 0.1‰ owing to the proximity to its formation region in the Southern Ocean. Where UCDW upwells, at approximately 55°S–60°S, it has a relatively high AOU and nitrate concentration, and nitrate $\delta^{15}N$ of 5.0‰ and $\delta^{18}O$ of 2.1‰, reflecting contributions of both low-$\delta^{15}N$ NADW nitrate and high-$\delta^{15}N$ IDW and Pacific Deep Water nitrate (Fripiat et al., 2019; Sigman, et al., 1999, 2000; Smart et al., 2015; Talley et al., 2011). In the Agulhas Current, the mean AOU and nitrate concentration in UCDW are 160.1 ± 7.6 μM and 30.7 ± 1.3 μM, respectively, and nitrate $\delta^{15}N$ and $\delta^{18}O$ are 5.5 ± 0.1‰ and 2.2 ± 0.1‰. The elevated nitrate $\delta^{15}N$ but similar $\delta^{18}O$ relative to UCDW at formation suggests the remineralization of organic matter with a relatively high $\delta^{15}N$ in the Subantarctic Zone where UCDW directly underlies Subantarctic Surface Water (Fripiat et al., 2019). In the western Mozambique Channel, the upper limit of UCDW has a slightly higher density than UCDW in the Agulhas Current (σ_2 = 36.6 kg.m^{-3} vs. 36.5 kg.m^{-3}, the former being ∼100 m deeper). In the channel, UCDW has a mean AOU, nitrate concentration, and nitrate $\delta^{15}N$ and $\delta^{18}O$ of 200.0 ± 8.1 μM, 34.6 ± 1.3 μM, 6.1 ± 0.1‰, and 2.5 ± 0.1‰, respectively. These values are higher than those measured for UCDW in the Agulhas Current, although we note that the Mozambique Channel samples were collected down to 1,500 m only (σ_2 = 36.7 kg.m^{-3}). Regardless, the higher AOU, nitrate concentration and isotope ratios suggest that UCDW in the Mozambique Channel has mixed with the overlying intermediate waters, which carry remineralization and denitrification signals generated in the Arabian basin (see Section 3.1.2). The presences of two overlying intermediate waters may also explain why UCDW in the channel occurs slightly deeper than in the Agulhas Current.

3.1.2. Intermediate Waters

There are two intermediate water masses in the southwest Indian Ocean, Antarctic Intermediate Water (AAIW) and Red Sea Water (RSW), which occupy a similar density range (27.0 kg.m^{-3} < σ_θ < 27.4 kg.m^{-3}; (Beal et al., 2006; Roman & Lutjeharms, 2007, 2009; Toole & Warren, 1993)). The stark differences in the salinity and AOU of AAIW and RSW evince their disparate formation histories (Figures 3–5; Tables 1 and 2).

AAIW is formed in the Polar Frontal Zone (at approximately 50°S–55°S) where surface waters are relatively fresh (Reid, 2003; Talley et al., 2011) and partial nitrate assimilation by phytoplankton produces relatively high $\delta^{15}N$ and $\delta^{18}O$ nitrate (Sigman et al., 1999, 2000; Smart et al., 2015). In the Indian sector of the Southern Ocean, AAIW has a nitrate concentration of 27.5 μM and $\delta^{15}N$ and $\delta^{18}O$ of 5.7 and 2.7‰, respectively (Fripiat et al., 2019). This water mass enters the Indian basin at around 60°E, its northward passage aided by the bathymetry of the Southwest Indian ridge (Fine, 1993). AAIW circulates within the subtropical gyre and subsequently enters the Agulhas Current, primarily through recirculation of the subtropical waters and to a lesser extent, through the South East Madagascar Current and Mozambique Channel (Beal et al., 2006; Fine, 1993). In the Agulhas Current and adjacent recirculating waters, mean AAIW salinity, nitrate concentration, and $\delta^{15}N$ and $\delta^{18}O$ are 34.6 ± 0.06 g.kg^{-1}, 28.3 ± 2.4 μM, 6.0 ± 0.1‰, and 2.6 ± 0.1‰, respectively. Thus, AAIW still bears the salinity minimum and high nitrate $\delta^{18}O$ imparted at formation, while its nitrate $\delta^{15}N$ is even higher. In the western Mozambique Channel, AAIW occupies a slightly lower and narrower density range (26.9 kg.m^{-3} < σ_θ < 27.1 kg.m^{-3}), sandwiched between two high-salinity and high-$\delta^{15}N$ nitrate water masses (Figures 3 and 4c inset). Here, its mean salinity, $\delta^{15}N$, and $\delta^{18}O$ (of 34.9 ± 0.02 g.kg^{-1}, 6.6 ± 0.1‰, and 3.0 ± 0.1‰, respectively) are considerably higher than in AAIW at formation and slightly higher than in the Agulhas Current and adjacent recirculating waters, while its nitrate concentration is lower (24.6 ± 2.7 μM). The higher $\delta^{15}N$ of AAIW nitrate in the southwest Indian Ocean compared to at formation is likely due to both mixing with RSW (see below) and remineralization of high-$\delta^{15}N$ organic matter produced in the subtropical surface waters overlying equatorward-flowing AAIW. In the latter case, the high-$\delta^{15}N$ organic matter derives from complete consumption of mode-water nitrate that is higher in $\delta^{15}N$ than AAIW nitrate (Fripiat et al., 2019; Rafter et al., 2013).

RSW is formed by strong evaporation over the northwest Indian Red Sea, where salinity is 40 g.kg^{-1} (Beal et al., 2000; Bower et al., 2000). This water mass is thus discernible throughout the Indian Ocean by a relative

salinity maximum (Talley et al., 2011). RSW flows through the Arabian Sea oxygen deficient zone and upon exiting, carries the elevated nitrate $\delta^{15}N$ and $\delta^{18}O$ imparted by denitrification (mean of 9.3 and 7.9‰, respectively, at times reaching 16‰; Figure 5a), along with a strong remineralization signal (AOU > 250 μM) (Brandes et al., 1998; Gaye et al., 2013; Martin & Casciotti, 2017). RSW enters the Agulhas Current primarily through the Mozambique Channel, with a purity of 30%–40% and transport volume of 1.4 Sv (Roman & Lutjeharms, 2009), as well as via the South East Madagascar Current at a significantly reduced purity and volume (~15% and 0.3 Sv) (Donohue & Toole, 2003; Roman & Lutjeharms, 2009). In the western Mozambique Channel, RSW (σ_θ = 27.1 kg.m^{-3} to σ_2 = 36.6 kg.m^{-3}) is discernible by a salinity maximum of 35.0 ± 0.03 g.kg^{-1}, AOU of 204.3 ± 15.9 μM, nitrate concentration of 32.9 ± 2.8 μM, and nitrate $\delta^{15}N$ and $\delta^{18}O$ of 6.6 ± 0.1‰ and 2.9 ± 0.1‰, respectively. Downstream in the Agulhas Current, the distribution of RSW is patchy due to seasonally variable transport from the Red Sea and Mozambique Channel, and takes the form of lenses and filaments (Beal et al., 2000; Roman & Lutjeharms, 2009).

In the western Mozambique Channel, RSW bears similarly elevated N and O isotope ratios to AAIW in the Agulhas Current (although generated through different mechanisms). However, we can identify RSW in the Agulhas Current because it occurs at a slightly higher density (i.e., deeper) than AAIW (σ_θ = 27.0–27.4 kg.m^{-3} vs. 27.45–27.55 kg.m^{-3}), near-coincident with UCDW that has a lower nitrate $\delta^{15}N$ and $\delta^{18}O$ than RSW (Table 1, Figure 4 insets, Figure 5b). Two RSW lenses are apparent in our data set, represented by few discrete measurements (n = 5 for the ASCA16 lens and n = 2 for the SWINGS lens; Text S2 in Supporting Information S1), which is unsurprising given the reduced purity and volume expected for RSW in this region (Roman & Lutjeharms, 2009). The ASCA16 lens is located between 34.1°S and 34.7°S and is characterized by a salinity of 34.7 ± 0.03 g.kg^{-1}, AOU of 164.3 ± 5.2 μM, nitrate concentration of 32.2 ± 0.3 μM, and nitrate $\delta^{15}N$ and $\delta^{18}O$ of 6.0 ± 0.0‰ and 2.6 ± 0.1‰, respectively (Table S1 in Supporting Information S1), while the SWINGS lens is located between 30.30°S and 30.66°S and has a salinity of 34.8 ± 0.03 g.kg^{-1}, AOU of 172.4 ± 7.5 μM, nitrate concentration of 31.6 ± 2.4 μM, and nitrate $\delta^{15}N$ of 5.9 ± 0.1‰ (Table S2 in Supporting Information S1).

The nitrate isotope ratios provide a means of identifying and quantifying RSW in the Agulhas Current since the $\delta^{15}N$ (and $\delta^{18}O$) of RSW nitrate is elevated relative to that of UCDW, by 0.4–0.5‰ (and by 0.4‰) (Table 1 and Figure 4 inset). Using a two-endmember mixing model, we can estimate the fraction (i.e., purity) of RSW in the Agulhas Current lenses, which together have a mean nitrate $\delta^{15}N$ of 5.9 ± 0.1‰. We set the $\delta^{15}N$ of the first endmember to the mean RSW nitrate $\delta^{15}N$ of 9.3 ± 0.3‰ measured in the Arabian Sea (Martin & Casciotti, 2017), while the second endmember is the $\delta^{15}N$ of UCDW nitrate at formation (5.0 ± 0.0‰; (Fripiat et al., 2019; Smart et al., 2015)). By mixing these two endmembers, we estimate the fraction of RSW in the Agulhas Current lenses to be approximately 21%. This value is consistent with the 10%–20% purity estimated previously for RSW in the Agulhas Current and adjacent waters using an optimum multi-parameter analysis that considered 15 data sets from the region and required seven input variables (Roman & Lutjeharms, 2009).

3.1.3. Sub-Thermocline Waters

Subantarctic Mode Water (SAMW; σ_θ = 26.4–27.0 kg.m^{-3}) is formed in the deep winter mixed layers north of the Subantarctic Front (approximately 45°S–50°S) and records partial phytoplankton nitrate assimilation in its isotope ratios, similar to AAIW (DiFiore et al., 2006; Fripiat et al., 2021; Rafter et al., 2013; Sigman et al., 1999, 2000). SAMW subducts and flows northwards in the interior of the subtropical gyres to eventually supply nutrients to most of the global ocean thermocline (Fripiat et al., 2021; Sarmiento et al., 2004).

Two types of SAMW occur in the South Indian Ocean: (a) SAMW that last ventilated west of 70°E (i.e., west of the Kerguelen Plateau) with a core density of 26.5 kg.m^{-3}, and (b) Southeast Indian SAMW (SEISAMW) that last ventilated east of the Kerguelen Plateau and has a higher core density of 26.8 kg.m^{-3} (Fine, 1993; Herraiz-Borreguero & Rintoul, 2011; Koch-Larrouy et al., 2010; McCartney, 1982; Wong, 2005). Both SAMW types can be reventilated through interaction with the base of the relatively deep winter mixed layers that occur in the southern reaches of the subtropical gyre, before circulating anticyclonically through the South Indian basin (Koch-Larrouy et al., 2010; Lu et al., 2021; Wong, 2005).

In the eastern Indian sector of the Southern Ocean (i.e., in the region where SEISAMW forms), nitrate $\delta^{15}N$ is 6.8‰ and $\delta^{18}O$ is 3.9‰ (Figure 5a; Fripiat et al., 2019). There are currently no nitrate isotope measurements of SAMW formed west of 70°E yet both types of SAMW reach the southwest Indian Ocean. SEISAMW is thought to enter via a longer route through the Mozambique Channel and South East Madagascar Current while SAMW,

formed more locally, enters through the subtropical recirculation (Beal et al., 2006; Donohue & Toole, 2003; Talley et al., 2011; Toole & Warren, 1993). The SAMW in the western Mozambique Channel is thus likely SEISAMW, with a mean AOU of 94.3 ± 4.6 μM and nitrate $\delta^{15}N$ and $\delta^{18}O$ of 6.8 ± 0.2‰ and 3.3 ± 0.2‰, respectively. In the Agulhas Current and adjacent recirculating waters, the SAMW is likely more locally formed, with a lower mean AOU (57.4 ± 4.4 μM), near-indistinguishable nitrate $\delta^{15}N$ (6.9 ± 0.1‰), and slightly higher nitrate $\delta^{18}O$ (3.5 ± 0.1‰) than SEISAMW in the western Mozambique Channel (Figure 3; Table 1). The higher AOU and lower nitrate $\delta^{18}O$ of SEISAMW in the channel evince a larger remineralization signal (i.e., more nitrification) than in the downstream Agulhas waters. This observation corroborates previous work suggesting that due to differences in circulation, SEISAMW in the western Mozambique Channel is older (i.e., has had more time to accumulate the products of remineralization) than SAMW directly supplied to the subtropical recirculation and subsequently, the Agulhas Current (Beal et al., 2006; Fine, 1993; Fine et al., 2008; Koch-Larrouy et al., 2010; Wong, 2005). In our ASCA16 data set, SAMW is apparent at the shallow shelf station (latitude = 33.34°S; red circles in Figure 4) in the high mean shelf nitrate $\delta^{15}N$ and $\delta^{18}O$ of 7.0 and 3.7‰ ($\Delta(15–18) = 3.4$‰), likely due to inshore upwelling (Leber et al., 2017; Russo et al., 2019).

3.1.4. Thermocline and Surface Waters

Thermocline waters: We identify two thermocline waters in the southwest Indian Ocean, Tropical Thermocline Water (TTW; σ_θ = 24.5–26.4 kg.m^{-3}) and Subtropical Thermocline Water (STTW; σ_θ = 25.5–26.4 kg.m^{-3}). These waters occupy a similar density range but have different formation histories, making them easily distinguishable by salinity and AOU, as well as by their physical partitioning across the Agulhas Current core (Figures 3–5; Table 1; Beal et al., 2006). TTW underlies Tropical Surface Water (TSW; σ_θ < 24.5 kg.m^{-3}), with both water masses forming in the warm, fresh tropical latitudes (approximately 5–25°S) where precipitation exceeds evaporation and fresh Indonesian Through Flow waters are supplied by the South Equatorial Current (SEC; Figure 1) (Gordon, 1987; Gordon et al., 1997; Wyrtki, 1971). STTW underlies Subtropical Surface Water (STSW; σ_θ < 25.5 kg.m^{-3}), with both water masses forming in the more saline subtropical gyre (25–35°S, east of 90°E) where evaporation exceeds precipitation (Beal et al., 2006; Gordon, 1987; Wyrtki, 1971). TTW is thus a comparatively fresh thermocline water mass (salinity of 35.4–35.6 g.kg^{-1}) compared to its subtropical counterpart (salinity >35.7 g.kg^{-1}) (Figures 2a and 3).

TTW is the only thermocline water mass in the western Mozambique Channel, with a salinity of 35.5 ± 0.05 g.kg^{-1}, AOU of 99.7 ± 10.1 μM, nitrate concentration of 10.9 ± 2.2 μM, and nitrate $\delta^{15}N$ and $\delta^{18}O$ of 6.0 ± 0.4‰ and 2.8 ± 0.4‰, respectively (Figures 3 and 4, Table 2). By the time TTW reaches the Agulhas Current, it is constrained to the inshore side of the current core (Figure 2). Here, it is slightly more saline (mean salinity of 35.6 ± 0.05 g.kg^{-1}), has a lower AOU and nitrate concentration (73.4 ± 13.6 μM and 7.8 ± 1.8 μM), and slightly lower nitrate $\delta^{15}N$ and $\delta^{18}O$ (5.8 ± 0.3‰ and 2.7 ± 0.4‰) than in the western Mozambique Channel, likely due to lateral entrainment of subtropical water by Mozambique Channel eddies as they propagate southwards. At formation, the nitrate $\delta^{15}N$ of STTW is 7.0 ± 0.1‰ and its $\delta^{18}O$ is 4.5 ± 0.1‰ (Figures 1 and 5a; Sigman & Fripiat, 2019). STTW enters the Agulhas Current through the subtropical gyre recirculation where it has a mean salinity of 35.7 ± 0.03 g.kg^{-1}, AOU of 28.3 ± 11.3 μM, and nitrate concentration of 3.0 ± 1.4 μM (Table 1). Its mean nitrate $\delta^{15}N$ and $\delta^{18}O$ of 4.9 ± 0.7‰ and 2.8 ± 0.8‰, respectively, are lower than at formation. Indeed, both thermocline waters have a lower nitrate $\delta^{15}N$ than their upstream endmembers and the underlying SAMW, suggesting local remineralization of low-$\delta^{15}N$ organic matter. This thermocline signal is similarly observed in summer (i.e., SWINGS and Text S4 in Supporting Information S1). STTW nitrate $\delta^{15}N$ is on average lower than that of TTW, 4.9 versus 5.8‰ (5.1 vs. 6.2‰ for the SWINGS data set), reaching a minimum of 4.2 versus 5.2‰. Thus, in the Agulhas Current, TTW is biogeochemically different from STTW and is characterized by a higher AOU, nitrate concentration, and nitrate $\delta^{15}N$.

Surface waters: At formation, TSW (σ_θ < 24.5 kg.m^{-3}) is particularly fresh (salinity <35.0 g.kg^{-1}). During the westward transit of TSW to the Mozambique Channel, the incorporation of Arabian Sea surface waters increase its salinity, such that in the western channel, TSW is characterized by salinities ≥35.3 g.kg^{-1} (mean of 35.4 ± 0.05 g.kg^{-1}; Figure 3 and Table 2) (DiMarco et al., 2002; Donohue & Toole, 2003; Wyrtki, 1971). TSW salinity is further increased to 35.6 ± 0.51 g.kg^{-1} inshore of the Agulhas Current (Figure 3 and Table 1), likely also due to the lateral entrainment of more saline STSW by southward propagating Mozambique Channel eddies. STSW (σ_θ < 25.5 kg.m^{-3}) is transported into the Agulhas Current via the subtropical gyre recirculation (DiMarco et al., 2002; Gründlingh et al., 1991). In the Agulhas Current and adjacent recirculating waters, STSW has a

relatively high salinity (mean of 35.7 ± 0.03 g.kg^{-1}) compared to TSW. Both TSW and STSW have a relatively low nitrate concentration of ∼1.0 μM and elevated nitrate $\delta^{15}N$ and $\delta^{18}O$, of >6.5‰ and >4.0‰, respectively, reaching values as high as 11.5 and 9.9‰ (Figures 3 and 4), due to photosynthetic nitrate assimilation (J. Granger et al., 2004, 2010; Sigman et al., 1999). The depth of the mixed layer, defined by vertical gradients in density and nitrate concentration (Figure 2), is largely coincident with the boundary of the surface waters (Figures 2b and 5b).

4. Discussion

We discuss the implications of the nitrate isotope distributions in the upper southwest Indian Ocean (σ_θ < 26.4 kg.m^{-3} or shallower than 500 m) in detail below. The southwestern region of the subtropical gyre (20–70°E) is characterized by highly retentive thermocline circulation that is largely dominated by waters from the Agulhas Return Current and is sometimes referred to as the southwest Indian subgyre (Figure 1; Grand, Measures, Hatta, Morton, et al., 2015; Lutjeharms & Ansorge, 2001; Ridgway & Dunn, 2007; Stramma & Lutjeharms, 1997). Hereafter, we will refer to the Agulhas Current (tropical and subtropical waters) and adjacent recirculating (subtropical) waters collectively as the "greater Agulhas region" (i.e., all stations sampled during ASCA16 and SWINGS).

4.1. Nitrogen Cycling in the Thermocline and Mixed Layer of the Greater Agulhas Region

Across the greater Agulhas region, upper thermocline and mixed-layer nitrate Δ(15–18) is low relative to underlying SAMW (Figure 4e). Above σ_θ = 26.0 kg.m^{-3}, mean nitrate Δ(15–18) is 1.6‰, reaching as low as −0.5‰, while SAMW nitrate Δ(15–18) is 3.4‰. Two processes can cause the Δ(15–18) of nitrate to decrease. The first is N_2 fixation, which lowers the $\delta^{15}N$ of thermocline nitrate more than its $\delta^{18}O$ through the introduction of low-$\delta^{15}N$ (i.e., ∼−1‰) organic matter (Carpenter et al., 1997; Hoering & Ford, 1960; Minagawa & Wada, 1986). The nitrate generated from the remineralization and nitrification of this newly fixed organic matter is similarly low in $\delta^{15}N$ while its $\delta^{18}O$, which is set by $\delta^{18}O_{H2O}$ (equal to ∼0‰) plus an isotopic offset, is ≥1.1‰ (Fawcett et al., 2015; Knapp et al., 2008; Lehmann et al., 2018; Marconi et al., 2019; Rafter et al., 2013; Sigman et al., 2005, 2009). The second process is partial nitrate assimilation occurring in the same water parcel as nitrification (Deman et al., 2021; Fawcett et al., 2015; Smart et al., 2015; Wankel et al., 2007). These co-occurring processes generate nitrate that is high in $\delta^{18}O$ relative to that initially removed by phytoplankton but leave nitrate $\delta^{15}N$ unchanged (since in net, N is neither gained nor lost from the water parcel; Fawcett et al., 2015; Rafter et al., 2013; Sigman et al., 2005, 2009). The signal of coupled nitrate assimilation and nitrification can be generated in situ (i.e., nitrate assimilation and nitrification co-occurring at the base of the euphotic zone; Fawcett et al., 2015) or as a result of partial nitrate assimilation in surface waters that then subduct and flow laterally along subsurface isopycnals where nitrification occurs (Deman et al., 2021; Fawcett et al., 2018). While both N_2 fixation and co-occurring nitrate assimilation and nitrification decrease the Δ(15–18) of nitrate, N_2 fixation also lowers its $\delta^{15}N$ (Figure 6a vs. Figure 6b).

4.1.1. Drivers of the Low Nitrate Δ(15–18) in the Upper Thermocline

Thermocline nitrate $\delta^{15}N$ across the greater Agulhas region, which ranges from 4.2 to 5.5‰, is low relative to sub-thermocline SAMW ($\delta^{15}N$ of 6.9‰), while its $\delta^{18}O$ ranges from 2 to 3‰ (also lower than the mean SAMW $\delta^{18}O$ of 3.5‰, but not to the same degree as the $\delta^{15}N$) (Figures 4c and 4d). As a result, nitrate Δ(15–18) decreases from 3.4 ± 0.1‰ in SAMW to a mean of 3.2 ± 0.3‰ in TTW and 2.1 ± 0.8‰ in STTW, reaching a minimum of −0.5‰ (Figure 4e and Table 1). The general coincidence of low-$\delta^{15}N$ and low-Δ(15–18) nitrate can be explained by N_2 fixation (Knapp et al., 2008; Lehmann et al., 2018; Rafter et al., 2013; Sigman et al., 2005). Since the dual isotopes of SAMW nitrate are both elevated and N_2 fixation lowers nitrate $\delta^{15}N$ more than its $\delta^{18}O$, the addition of newly fixed nitrate to the Agulhas thermocline will drive the nitrate data above the 1:1 line in a plot of $\delta^{18}O$ versus $\delta^{15}N$ (i.e., toward a lower Δ(15–18); Figure 6a). This trend is evident in the subtropical thermocline between σ_θ = 25.5 kg.m^{-3} and 26.4 kg.m^{-3} and in the tropical thermocline between σ_θ = 24.5 kg.m^{-3} and 26.4 kg.m^{-3} (orange arrow in Figure 6c).

Upper thermocline nitrate Δ(15–18) continues to decline toward the base of the mixed layer, which broadly coincides with the 25.5 kg.m^{-3} and 24.5 kg.m^{-3} isopycnals for subtropical and tropical waters, respectively (Figures 4e and 6c). Here, subtropical water nitrate $\delta^{18}O$ rises by ∼1.5‰ while its $\delta^{15}N$ remains relatively constant between 4.5 and 5.0‰ (mean of 4.8 ± 0.3‰). Nitrate Δ(15–18) thus decreases from 2.1 ± 0.5‰ to

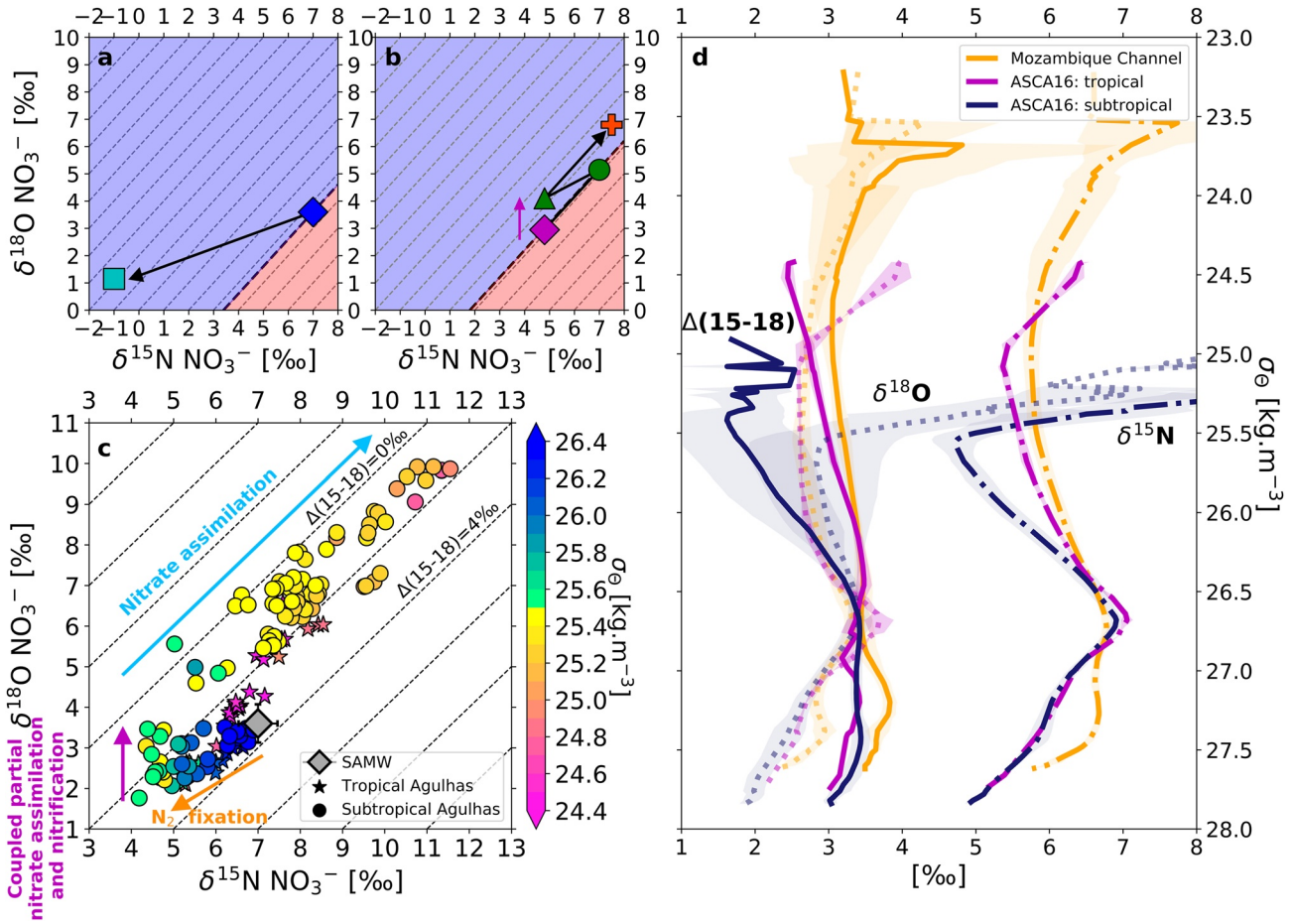

Figure 6. Coupled N and O isotope dynamics in the greater Agulhas region. Panels (a, b, and c) show nitrate $\delta^{18}O$ versus $\delta^{15}N$ [‰], with dashed diagonal contours indicating nitrate Δ(15–18) [‰]. Panel (a) shows how N_2 fixation lowers thermocline nitrate $\delta^{15}N$ more than its $\delta^{18}O$, thereby lowering Δ(15–18). Panel (b) shows how in net, coupled partial nitrate assimilation (magenta diamond to green circle) and nitrification (green circle to green triangle) cause the $\delta^{18}O$ of nitrate to rise while its $\delta^{15}N$ remains unchanged (net effect indicated by the vertical magenta arrow). This mechanism lowers the Δ(15–18) of nitrate at the base of the greater Agulhas region mixed layer and when that nitrate is subsequently assimilated in surface waters (green triangle to red plus), its Δ(15–18) remains unchanged (i.e., low) even as its $\delta^{15}N$ and $\delta^{18}O$ rise. In panels (a and b), the blue shading indicates values of nitrate Δ(15–18) that are lower than the source nitrate while the red shading indicates higher nitrate Δ(15–18). Panel c shows the ASCA16 data colored by potential density (σ_θ) [kg.m^{-3}] with arrows and text indicating the effect on the nitrate isotope ratios of the various processes outlined above and discussed in the text. The gray diamond indicates the mean, concentration-weighted $\delta^{18}O$ and $\delta^{15}N$ of SAMW with propagated error shown by the capped bars. Panel (d) shows mean density profiles of nitrate $\delta^{15}N$ (dash-dotted line), $\delta^{18}O$ (opaque dotted line), and Δ(15–18) (solid line) [‰], with ±1 SD represented by the opaque shading. The profile colors indicate the regions from which the data were collected (see legend), with the Mozambique Channel data included to represent the tropical endmember to the Agulhas Current.

<0‰ (Figure 6c). Analogously, tropical water nitrate Δ(15–18) declines from 3.2 ± 0.3‰ to <2‰. A similar trend was observed at the Bermuda Atlantic Time-series Study (BATS) site where a 3.4‰ rise in nitrate $\delta^{18}O$ below the euphotic zone coincident with little change in nitrate $\delta^{15}N$ was explained by partial nitrate assimilation and nitrification mainly co-occurring in situ (Fawcett et al., 2015). We similarly attribute the low nitrate Δ(15–18) at the base of mixed layer in the greater Agulhas region to these co-occurring processes. The coincidence of partial nitrate assimilation and nitrification will drive shallow nitrate vertically above thermocline nitrate in $\delta^{18}O$ versus $\delta^{15}N$ space (i.e., above the 1:1 line and toward lower Δ(15–18); purple diamond to green triangle in Figure 6b and purple arrows in Figures 6b and 6c). The signal is likely generated predominantly in situ, akin to at BATS, with some portion possibly transported from the Subantarctic Southern Ocean (i.e., partial nitrate assimilation in Subantarctic surface waters followed by nitrification that occurs once these waters subduct and flow northwards). The combination of (a) partial nitrate assimilation and nitrification at the base of the mixed layer and (b) the introduction of newly fixed nitrate into the thermocline following surface N_2 fixation will vertically decouple the mean nitrate $\delta^{15}N$ minimum (deeper) from the mean nitrate Δ(15–18) minimum (shallower), as we observe (Figure 6d).

4.1.2. Phytoplankton Nitrate Assimilation Dominates the Mixed Layer Nitrogen Cycle

In the mixed layer of the greater Agulhas region, the linear relationship of $\delta^{18}O$ and $\delta^{15}N$ yields an approximately invariant $\Delta(15–18)$ that averages $1.2 \pm 0.5‰$ (green triangle to red cross in Figure 6b; blue arrow in Figure 6c). This pattern indicates that assimilation by phytoplankton is the dominant process acting on the surface nitrate pool (Fawcett et al., 2015; J. Granger et al., 2004, 2010; Rohde et al., 2015). The near-invariant nitrate $\Delta(15–18)$ also shows that nitrification does not occur in surface waters at significant rates during winter relative to the upward supply of subsurface nitrate (DiFiore et al., 2009; Fawcett et al., 2015; Peng et al., 2018). A similar condition is expected in spring through autumn when the mixed layer shoals and receives more light, which can directly inhibit nitrification (Merbt et al., 2012; R. Olson, 1981) and will favor the growth of phytoplankton that outcompete nitrifiers for ammonium (J. Smith et al., 2014; Ward, 1985). Since nitrate produced by mixed layer nitrification constitutes a regenerated rather than a new source of N to phytoplankton (Dugdale & Goering, 1967; Yool et al., 2007), its restriction to the waters below the mixed layer implies that the combined rate of nitrate assimilation and N_2 fixation can be used to approximate carbon export from Agulhas surface waters.

4.2. N_2 Fixation in the South Indian Ocean

4.2.1. Evidence of N_2 Fixation in the Greater Agulhas Region

We attribute the low $\delta^{15}N$ of thermocline nitrate across the greater Agulhas region to N_2 fixation. However, this signal could theoretically derive from three other processes. The first is the deposition of atmospheric N, which is generally low in $\delta^{15}N$ (-14 to $2‰$; Altieri et al., 2021). However, the mean modeled N deposition rate over the southwest Indian Ocean of 0.14 g $N.m^{-2}.a^{-1}$ (Jickells et al., 2017; Okin et al., 2011; Somes et al., 2016) is on average far too low to account for the low $\delta^{15}N$ of its thermocline nitrate (Text S5 in Supporting Information S1).

The second process that could decrease thermocline nitrate $\delta^{15}N$ is the lateral advection of high-$\delta^{15}N$ nitrate and/or dissolved organic N (DON) out of the greater Agulhas region while low-$\delta^{15}N$ organic matter is retained and remineralized in the thermocline (Lehmann et al., 2018; Rafter et al., 2013). However, inorganic N is the primary limiting nutrient in Agulhas surface waters, such that any nitrate supplied to the mixed layer should be rapidly consumed by phytoplankton, leaving little opportunity for partially assimilated, high-$\delta^{15}N$ nitrate to be advected away. Additionally, there is no discernible surface gradient in the DON concentration across the greater Agulhas region (Letscher et al., 2013), implying that significant lateral advection of DON (regardless of its $\delta^{15}N$, which is unknown) is unlikely. Furthermore, the tendency of the anticyclonic subgyre is to retain and downwell its shallow waters, such that even if nitrate were left unconsumed for a short period and/or high-$\delta^{15}N$ DON were produced, neither N species is likely to be transported out of the greater Agulhas region at significant rates.

The third process that could decrease thermocline nitrate $\delta^{15}N$ involves isotope fractionation during DON degradation. Shallow DON $\delta^{15}N$ profiles from some oligotrophic regions suggest preferential remineralization of ^{14}N during DON degradation (Knapp et al., 2018; Zhang et al., 2020), which could contribute low-$\delta^{15}N$ N to the thermocline (Zhang et al., 2020). The vertical gradients in the (limited) existing DON $\delta^{15}N$ data are variable and inconsistent however ((Zhang et al., 2020) and references therein), making estimates of the DON degradation isotope effect uncertain. Nevertheless, the thermocline nitrate-$\delta^{15}N$ minimum observed in the shallowest subsurface (i.e., below the euphotic zone) in many oligotrophic regions is typically held within the low concentration of nitrate that characterizes the top of the nitracline (Figures 4b and 4c). Accordingly, even a relatively small quantity ($\sim$1–2 μM) of DON-derived low-$\delta^{15}N$ N, if produced with an isotope effect of $\sim 5‰$ (Zhang et al., 2020), could be important in the shallowest component of the nitrate-$\delta^{15}N$ minimum. However, below the top of the nitracline where the nitrate concentrations rapidly increase with depth, DON degradation is too small of a nitrate source to explain the still-low thermocline nitrate $\delta^{15}N$. N_2 fixation must therefore play a dominant role in decreasing the $\delta^{15}N$ of thermocline nitrate. One complementary source of support for this interpretation comes from paleoceanographic records. Foraminifera-bound N isotope measurements suggest that, in both the North Atlantic and the South China Sea, the shallow thermocline nitrate $\delta^{15}N$ minimum has undergone proportionally large changes over glacial cycles; such changes are consistent with N_2 fixation, not isotope fractionation during organic N degradation, as the origin of the $\delta^{15}N$ minimum (Ren et al., 2009, 2017; Straub et al., 2013). In any case, future work will pursue the role of DON in the greater Agulhas region.

A final consideration is that in subtropical waters, low-$\delta^{15}N$ N also resides in the suspended particulate organic nitrogen (PON) pool (Altabet, 1988; Knapp et al., 2005, 2011). Suspended PON can be mixed down into the

shallow subsurface where it will be remineralized to low-$\delta^{15}N$ nitrate, potentially lowering the $\delta^{15}N$ of the thermocline nitrate pool. However, suspended PON represents a very small fraction of the total N pool (Fawcett et al., 2011) and thus has little capacity to change the $\delta^{15}N$ of subsurface nitrate (Knapp et al., 2005; Zhang et al., 2020).

Our conclusion that N_2 fixation occurs locally in the greater Agulhas region is consistent with previous observations. First, diazotrophs have been observed during the late-summer bloom that occurs irregularly to the southeast of Madagascar (Poulton et al., 2009), as well as within and south of the Mozambique Channel (Huggett & Kyewalyanga, 2017; Karlusich et al., 2021), with surface N_2 fixation rates of 2–18 $nM.d^{-1}$ measured southeast of Madagascar during the most recent (2020) late-summer bloom (Metzl et al., 2022). Second, one third of the thermocline nitrate at the north-eastern edge of the greater Agulhas region (~23°S, 70°E; Figure 1) has previously been estimated to be newly fixed based on subsurface nutrient N:P ratios (Harms et al., 2019). Here, the $\delta^{15}N$ of thermocline nitrate, which was measured to average 5.2 ± 1.1‰, and the mean AOU and nitrate concentrations of 27.9 ± 10.5 μM and 1.6 ± 1.3 μM, respectively, are remarkably similar to those of STTW in our data sets (Table 1) (Harms et al., 2019), strongly suggesting that newly fixed nitrate is retained in the greater Agulhas region. Third, the mean N* (= $[NO_3^-] - 16 \times [PO_4^{3-}]$; Gruber & Sarmiento, 1997) of −2.0 ± 0.5 μM in the Agulhas thermocline (N* in TTW = −2.3 ± 0.3 μM and in STTW = −1.8 ± 0.4 μM) is higher than that in underlying SAMW (mean N* of −2.7 ± 0.4 μM; data from WOCE IO6; Figure 4f), consistent with the addition of N in stoichiometric excess of phosphorus (P), which is characteristic of N_2 fixation (Deutsch et al., 2007; Marconi et al., 2017; Marshall et al., 2022). Importantly, a comparison of the 0–100 m vertical gradient in dissolved organic P recently measured in the greater Agulhas region (Liang et al., 2022) with that of DON from other regions (0.06–0.08 μM vs. 0.5–1 μM; (Zhang et al., 2020) and references therein) suggests that dissolved organic matter degradation occurs at or below the Redfield ratio (i.e., <16:1; Redfield et al., 1963). As such, N_2 fixation must be the dominant cause of the elevated N* in the thermocline of the greater Agulhas region even if DON degradation contributes to lowering its nitrate $\delta^{15}N$.

4.2.2. Quantifying Local N_2 Fixation in the Greater Agulhas Region

We use a one-box model to provide two estimates of the local newly fixed nitrate flux. Our approach incorporates the flux of nutrients, sinking organic matter, and N isotope ratios into and out of the upper waters (i.e., upper 400 m, which approximately includes the surface and thermocline waters) of the greater Agulhas region. The one-box model is governed by four steady-state equations (Equations 1–4) (Figure 7). Equation 1 expresses the water volume fluxes in Sv, with the tropical and subtropical source endmembers denoted as $_{Trop}$ and $_{Subtrop}$, and the flux out of the greater Agulhas region denoted as $_{Agulhas}$. Equations 2–4 express the P, N, and $\delta^{15}N$ fluxes into and out of the upper Agulhas waters, and include the organic matter sinking fluxes ($_{Sinking}$; in $mmol.m^{-2}.a^{-1}$) out of the base of the thermocline at 400 m. The sinking fluxes are independent of the water volume fluxes. Equations 3 and 4 additionally include a newly fixed nitrate flux (denoted as $_{Newly\ fixed}$), which is also independent of the water volume fluxes.

First, we assume that the water volume fluxes into and out of the greater Agulhas region are in steady-state, at least over the residence time of the thermocline (Equation 1). While this residence time is uncertain, proxies for water mass age suggest that the thermocline waters are between 2 and 6 years old (Fine et al., 2008; Karstensen & Tomczak, 1997; McDonagh et al., 2005); we use a conservative thermocline residence time of 4 years (i.e., since Agulhas thermocline waters are older than 2 and younger than 6 years, the maximum possible residence time is 4 years (Fine et al., 2008)). The volume of the upper Agulhas region is estimated by multiplying the surface area, taken to be the highly retentive region within the 18 m climatological dynamic height contour (Figure 1) of 7.3×10^{12} m^2, by the depth of the base of the thermocline (i.e., 400 m). The volume flux out of the upper Agulhas region is then computed by dividing its volume by the thermocline residence time (= 23.2 Sv) (Equation 1a). There are no estimates of the relative contributions of the source waters to the greater Agulhas region, so we use the proportions available for the Agulhas Current. The Mozambique Channel supplies only Tropical waters, contributing 22% ± 5% of the Agulhas waters (Beal et al., 2015; Ridderinkhof et al., 2010). The South East Madagascar Current contributes largely Subtropical waters, although ~20% of these waters derive from the northern/tropical Indian Ocean (Roman & Lutjeharms, 2009). We therefore assign 20% of the 24% ± 12% that the South East Madagascar Current contributes to the Agulhas waters (Beal et al., 2015; Ponsoni et al., 2016) to Tropical waters and the remaining 80% to Subtropical waters. The subtropical recirculation supplies only Subtropical waters and contrib-

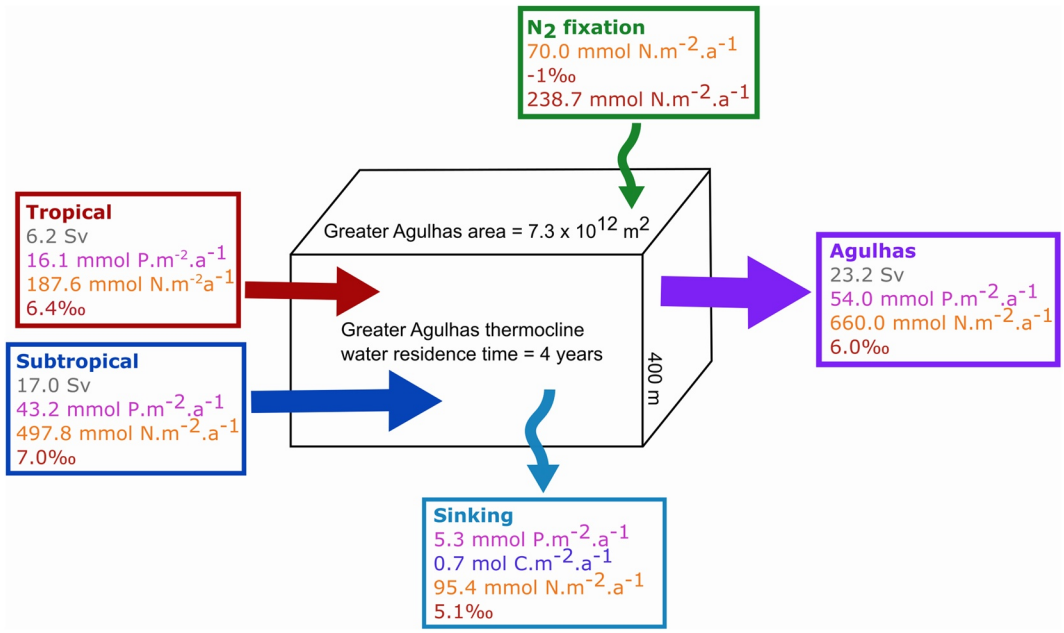

Figure 7. Estimating the newly fixed nitrate flux into the greater Agulhas region. Schematic of our one-box model showing the volume fluxes of water (gray text in Sv), phosphorus (pink text in mmol.m^{-2}.a^{-1}), nitrogen (orange text in mmol.m^{-2}.a^{-1}), and nitrogen δ^{15}N (red text in ‰) into and out of the upper 400 m of the greater Agulhas region (see Section 4.2.2 for more detail). The upper water column (mixed layer and thermocline) of the greater Agulhas region is represented by the black box, with a surface area of 7.3×10^{12} m^2, residence time of 4 years, and thermocline depth of 400 m. There are two source water inputs, Tropical (red box and arrow) and Subtropical (blue box and arrow), and one output, the Agulhas waters (purple box and arrow). The sinking flux (cyan box and arrow) at the base of the thermocline represents a non-hydrographic nutrient loss from the upper 400 m of the greater Agulhas region (as organic matter). N_2 fixation (green box and arrow) constitutes a non-hydrographic N gain.

utes the remaining 54% ± 17% to the Agulhas waters (Beal et al., 2015; Ponsoni et al., 2016; Ridderinkhof et al., 2010). In sum, the greater Agulhas region comprises 26.8% ± 6% Tropical waters (22% + 4.8%) and 73.2% ± 21% Subtropical waters (54% + 19.2%). The Tropical source water flux into the Agulhas region (Equation 1b) is thus 6.2 ± 1.4 Sv and the Subtropical source water flux (Equation 1c) is 17.0 ± 4.9 Sv (gray values in Figure 7).

$$\text{Volume flux}_{\text{Agulhas}} = \text{Volume flux}_{\text{Trop}} + \text{Volume flux}_{\text{Subtrop}} \quad (1)$$

$$\text{Volume flux}_{\text{Agulhas}} = \left(\text{Area}_{\text{Agulhas}} \times \text{Thermocline depth}_{\text{Agulhas}}\right) \div \text{Thermocline residence time}_{\text{Agulhas}} \quad (1a)$$

$$\text{Volume flux}_{\text{Trop}} = \left(26.8\% \times \text{Volume flux}_{\text{Agulhas}}\right) \quad (1b)$$

$$\text{Volume flux}_{\text{Subtrop}} = \left(73.2\% \times \text{Volume flux}_{\text{Agulhas}}\right) \quad (1c)$$

Second, we balance the P fluxes into and out of the upper Agulhas region (Equation 2). We multiply the mean phosphate concentrations measured in the Agulhas region and the Tropical and Subtropical source regions by their respective volume fluxes (Equation 1) and then solve for the flux of organic P out of the base of the thermocline. We use phosphate concentration data from three WOCE transects that sampled the endmember regions (small gray circles in Figure 1; Text S6 in Supporting Information S1). The mean phosphate concentration measured in the greater Agulhas region (IO6) is 0.54 ± 0.3 μM, at the Tropical source (IO4) is 0.60 ± 0.3 μM, and at the Subtropical source (IO8) is 0.59 ± 0.3 μM. The resulting phosphate flux for the Agulhas water is 54.0 mmol.m^{-2}.a^{-1} (Equation 2a), for the Tropical water is 16.1 mmol.m^{-2}.a^{-1} (Equation 2b), and for the Subtropical water is 43.2 mmol.m^{-2}.a^{-1} (Equation 2c). Using these values, we calculate an organic P sinking flux of 5.3 mmol P.m^{-2}.a^{-1} (pink values in Figure 7).

$$\text{Phosphate flux}_{\text{Trop}} + \text{Phosphate flux}_{\text{Subtrop}} = \text{Phosphate flux}_{\text{Agulhas}} + \text{Organic P flux}_{\text{Sinking}} \quad (2)$$

$$\text{Phosphate flux}_{\text{Agulhas}} = \text{Phosphate concentration}_{\text{Agulhas}} \times \text{Volume flux}_{\text{Agulhas}} \quad (2a)$$

$$\text{Phosphate flux}_{\text{Trop}} = \text{Phosphate concentration}_{\text{Trop}} \times \text{Volume flux}_{\text{Trop}} \quad (2b)$$

$$\text{Phosphate flux}_{\text{Subtrop}} = \text{Phosphate concentration}_{\text{Subtrop}} \times \text{Volume flux}_{\text{Subtrop}} \quad (2c)$$

Multiplying the organic P sinking flux by 128.6:1, the average measured C:P ratio of particulate organic matter in the greater Agulhas region (Copin-Montegut & Copin-Montegut, 1978; Martiny et al., 2013), suggests a flux of organic carbon from the base of the thermocline of 0.7 mol $C.m^2.a^{-1}$. For comparison, the mean organic carbon flux out of the seasonal mixed layer (i.e., net community production; NCP) at subtropical sites such as BATS and station ALOHA in the subtropical North Pacific is 2.5–3.8 mol $C.m^{-2}.a^{-1}$ ((Emerson, 2014) and references therein). We expect our sinking flux estimate to be lower than these values of NCP given the greater depth of the Agulhas region thermocline (i.e., 400 m) than the mixed layer at BATS and station ALOHA, along with the fact that a P-based carbon flux excludes sinking material deriving from N_2 fixation. Nonetheless, that our sinking flux is only an order of magnitude lower than NCP at BATS and station ALOHA is reassuring and validates our steady-state assumption and volume flux estimates.

Third, we balance the N fluxes into and out of the upper Agulhas region using the nutrient concentration data to estimate the generation of newly fixed nitrate (i.e., nitrate from the nitrification of organic N that was produced by new N_2 fixation) (Equation 3). We multiply the nitrate concentrations from the three WOCE transects by their respective volume fluxes (Equation 1). The mean nitrate concentration measured in the Agulhas (IO6) is 6.6 ± 5.0 μM, at the Tropical source (IO4) is 7.0 ± 4.7 μM, and at the Subtropical source (IO8) is 6.8 ± 4.2 μM. The resulting nitrate flux for Agulhas waters is 660.0 $mmol.m^{-2}.a^{-1}$ (Equation 3a), for Tropical water is 187.6 $mmol.m^{-2}.a^{-1}$ (Equation 3b), and for Subtropical water is 497.8 $mmol.m^{-2}.a^{-1}$ (Equation 3c). Multiplying the P-based organic sinking flux by the mean measured N:P of particulate organic matter in the region (average of 18.1:1; Copin-Montegut & Copin-Montegut, 1978; Martiny et al., 2013) yields a flux of organic N out of the thermocline of 95.4 mmol $N.m^{-2}.a^{-1}$ (Equation 3d).

$$\text{Nitrate flux}_{\text{Trop}} + \text{Nitrate flux}_{\text{Subtrop}} + \text{Nitrate flux}_{\text{Newly-fixed}} = \text{Nitrate flux}_{\text{Agulhas}} + \text{Organic N flux}_{\text{Sinking}} \quad (3)$$

$$\text{Nitrate flux}_{\text{Agulhas}} = \text{Nitrate concentration}_{\text{Agulhas}} \times \text{Volume flux}_{\text{Agulhas}} \quad (3a)$$

$$\text{Nitrate flux}_{\text{Trop}} = \text{Nitrate concentration}_{\text{Trop}} \times \text{Volume flux}_{\text{Trop}} \quad (3b)$$

$$\text{Nitrate flux}_{\text{Subtrop}} = \text{Nitrate concentration}_{\text{Subtrop}} \times \text{Volume flux}_{\text{Subtrop}} \quad (3c)$$

$$\text{Organic N flux}_{\text{Sinking}} = \text{Organic P flux}_{\text{Sinking}} \times \text{Organic N:P} \quad (3d)$$

$$\text{Nitrate flux}_{\text{Newly-fixed}} = \left(\text{Nitrate flux}_{\text{Agulhas}} + \text{Organic N flux}_{\text{Sinking}}\right) - \left(\text{Nitrate flux}_{\text{Trop}} + \text{Nitrate flux}_{\text{Subtrop}}\right) \quad (3e)$$

Substituting Equations 3a–3d into Equation 3 (as represented by Equation 3e) yields an estimate of the flux of newly fixed nitrate into the greater Agulhas region of 70.0 ± 84.7 mmol $N.m^{-2}.a^{-1}$ (orange values in Figure 7).

We can alternately estimate the flux of newly fixed nitrate into the greater Agulhas region using the N isotope data (Equation 4). We multiply the N fluxes from Equations 3a–3d by their respective $\delta^{15}N$ endmembers (Text S7 in Supporting Information S1). The mean concentration-weighted nitrate $\delta^{15}N$ for the Agulhas region is 6.0 ± 1.0‰ (taken from ASCA16; Equation 4a), for the Tropical waters is 6.4 ± 0.7‰ (taken from IIEO2; Equation 4b), and for the Subtropical waters is 7.0 ± 0.2‰ (taken from IO8, see Text S7 in Supporting Information S1; Sigman & Fripiat, 2019; Equation 4c). While N_2 fixation may occur in the South Equatorial Current, between the IO8 sampling site and the greater Agulhas region, there is only one nitrate $\delta^{15}N$ profile available in these waters (from 15°S, 74°E, Figure 1; Harms et al., 2019) and it shows no evidence of N_2 fixation. The relatively low nitrate $\delta^{15}N$ of the Tropical water indicates that N_2 fixation likely occurs in and/or upstream of the Mozambique Channel (i.e., in the northern tropical waters). However, the Tropical water nitrate $\delta^{15}N$ (of 6.4‰) is not low enough to yield the low nitrate $\delta^{15}N$ measured in the Agulhas waters (of 6.0‰), confirming that some amount of the signal must be generated by in situ N_2 fixation. There are no measurements of the $\delta^{15}N$ of sinking organic N in the Agulhas Current region; however, the sub-euphotic zone nitrate $\delta^{15}N$ can be used to estimate this term as it records the $\delta^{15}N$ of organic matter remineralized immediately below the surface layer (i.e., following its sinking out of the

euphotic zone). We thus set the $\delta^{15}N$ of sinking organic N to the mean sub-euphotic zone ($\sigma_\theta = 25.5–25.6$ kg.m^{-3}) nitrate $\delta^{15}N$ measured across the Agulhas region, of 5.1 ± 0.7‰ (Equation 4d).

$$\begin{aligned}\delta^{15}\mathrm{N\ nitrate\ flux_{Trop}} + \delta^{15}\mathrm{N\ nitrate\ flux_{Subtrop}} + \delta^{15}\mathrm{N\ nitrate\ flux_{Newly\text{-}fixed}} \\ = \delta^{15}\mathrm{N\ nitrate\ flux_{Agulhas}} + \delta^{15}\mathrm{N\ Organic\ N\ flux_{Sinking}}\end{aligned} \quad (4)$$

$$\delta^{15}\mathrm{N\ Nitrate\ flux_{Agulhas}} = \mathrm{Nitrate\ flux_{Agulhas}} \times \delta^{15}\mathrm{N_{Agulhas}} \quad (4a)$$

$$\delta^{15}\mathrm{N\ Nitrate\ flux_{Trop}} = \mathrm{Nitrate\ flux_{Trop}} \times \delta^{15}\mathrm{N_{Trop}} \quad (4b)$$

$$\delta^{15}\mathrm{N\ Nitrate\ flux_{Subtrop}} = \mathrm{Nitrate\ flux_{Subtrop}} \times \delta^{15}\mathrm{N_{Subtrop}} \quad (4c)$$

$$\delta^{15}\mathrm{N\ Organic\ N\ flux_{Sinking}} = \mathrm{Organic\ N\ flux_{Sinking}} \times \delta^{15}\mathrm{N_{subeuphotic\ zone}} \quad (4d)$$

$$\mathrm{Nitrate\ flux_{Newly\text{-}fixed}} = \frac{\left(\delta^{15}\mathrm{N\ flux_{Agulhas}} + \delta^{15}\mathrm{N\ flux_{Sinking}}\right) - \left(\delta^{15}\mathrm{N\ flux_{Trop}} + \delta^{15}\mathrm{N\ flux_{Subtrop}}\right)}{\delta^{15}\mathrm{N_{N2\ fixation}}} \quad (4e)$$

Substituting Equations 4a–4d into Equation 4 (to yield Equation 4e) and setting the $\delta^{15}N$ of newly fixed nitrate to −1‰ (Carpenter et al., 1997; Hoering & Ford, 1960; Minagawa & Wada, 1986) provides a second estimate of the newly fixed nitrate flux into the greater Agulhas region of 238.7 ± 157.5 mmol N.m^{-2}.a^{-1} (red values in Figure 7). The sensitivity of this flux to the $\delta^{15}N$ of each endmember and the uncertainties associated with all fluxes, derived through error propagation of the volume fluxes, are reported in Text S8 in Supporting Information S1.

Above, we derive two estimates of the newly fixed nitrate flux to the greater Agulhas region, of 70.0 and 238.7 mmol N.m^{-2}.a^{-1}. We consider the nutrient concentration-based estimate (Equation 3e) to be the lower limit of the N_2 fixation rate and the N isotope-based estimate (Equation 4e) to be the upper limit. In particular, the N isotope-based estimate is likely too high. The subtropical nitrate $\delta^{15}N$ endmember is poorly constrained as the available data are from substantially upstream of the subtropical Agulhas source region (Figure 1). As such, the subtropical $\delta^{15}N$ endmember does not include the signal of any N_2 fixation occurring en route to the subtropical source region. Coincident nutrient and N isotope data from the subtropical waters nearer the greater Agulhas region would better constrain our estimate. Additionally, our N isotope budget does not account for DON cycling because the $\delta^{15}N$ of DON in our region is unknown. Since DON degradation has the potential to supply low-$\delta^{15}N$ N to the thermocline nitrate pool (see Section 4.2.1; Zhang et al., 2020), its exclusion from our budget could lead us to overestimate the N_2 fixation rate from the N isotopes. For its part, the nutrient concentration-based estimate of N_2 fixation may be biased low, for reasons described in Section 4.2.3.

Notwithstanding these uncertainties, the fluxes of newly fixed nitrate calculated using the box model scale to an areal N_2 fixation rate for the greater Agulhas region of between 7.2 and 24.5 Tg N.a^{-1}, and a daily N_2 fixation rate of between 192 and 654 μmol N.m^{-2}.d^{-1}. Our daily rates are comparable to euphotic zone-integrated N_2 fixation rates that we measured along the ASCA transect in winter 2018, of 28–236 μmol N.m^{-2}.d^{-1} (Text S9 in Supporting Information S1), as well as to estimates from other subtropical regions (Landolfi et al., 2018). Our analysis indicates that N_2 fixation in the greater Agulhas region could contribute 28%–94% of the whole Indian Ocean N gain estimated by models (Deutsch et al., 2007; Landolfi et al., 2018; Wang et al., 2019).

4.2.3. Controls on N_2 Fixation in the South Indian Ocean

N_2 fixation is hypothesized to be controlled by the availability of excess P relative to N (Deutsch et al., 2007), the supply of bioavailable iron (Moore et al., 2009; Shiozaki et al., 2014), or both (Cerdan-Garcia et al., 2022; Held et al., 2020; Marshall et al., 2022; Mills et al., 2004; Singh et al., 2017; Weber & Deutsch, 2014). The surface waters of the Indian Ocean host a P excess (>0.1 μM; Deutsch et al., 2007; Garcia et al., 2018), which is largely generated in the Arabian Sea where denitrification removes fixed N but not P (Deutsch et al., 2007; DeVries et al., 2013). More locally, the western Mozambique Channel shelf appears to supply P in stoichiometric excess of N to the overlying waters (P excess of >0.3 μM; Figure S9 in Supporting Information S1), potentially augmenting the basin-wide P excess. In calculating the nutrient concentration-based N_2 fixation rate, we are unlikely to have fully accounted for this local P excess (i.e., low N* input) in our P and N budgets, leading to an underestimation of N_2 fixation. Upper ocean dissolved iron measurements from across the Indian basin, albeit limited, reveal generally higher concentrations in the northern versus southern basin (0.1–1.3 nM vs. 0.05–0.5 nM) and near the south-western and south-eastern

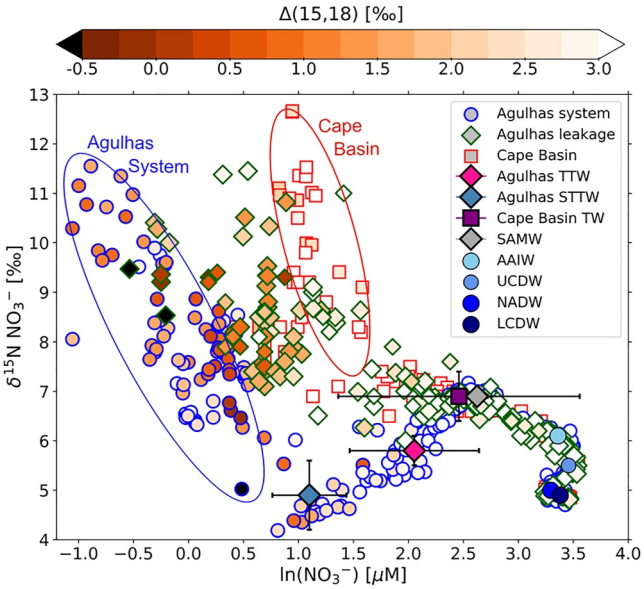

Figure 8. Tracking Agulhas leakage into the South Atlantic Ocean. Data from ASCA16 and the subtropical South Atlantic plotted in nitrate $\delta^{15}N$ [‰] versus $\ln([NO_3^-])$ [μM] space (i.e., "Rayleigh space"), with symbol color indicating nitrate Δ(15–18) [‰]. Symbol shape and outline-color indicate the sampling region, except for the bold diamond markers outlined in black, which show the mean $\ln([NO_3^-])$ and concentration-weighted nitrate $\delta^{15}N$ measured for Subantarctic Mode Water (SAMW; gray), Agulhas Subtropical Thermocline Water (STTW; blue), and Agulhas Tropical Thermocline Water (TTW; pink), as well as the purple square, which shows Cape Basin Thermocline Water (TW). In addition, the mean $\ln([NO_3^-])$ and concentration-weighted nitrate $\delta^{15}N$ are shown for Antarctic Intermediate Water (AAIW), Upper Circumpolar Deep Water (UCDW), North Atlantic Deep Water (NADW), and Lower Circumpolar Deep Water (LCDW), as measured in the Agulhas region. Four data sets that sampled both "background" Cape Basin conditions (squares outlined in red) and Agulhas leakage (diamonds outlined in green) are included on the plot: VOY016 cruise (Smart et al., 2020), SAMBA: South Atlantic MOC Basin-wide Array 2015 (Marconi et al., 2017) and 2017 (R. Granger et al., 2023), and VOY03 cruise (Smart et al., 2015).

margins versus the south-central basin (reaching 1.4 vs. 0.2 nM) (Chinni & Singh, 2022; Grand, Measures, Hatta, Hiscock, et al., 2015; Grand, Measures, Hatta, Morton, et al., 2015; Nishioka et al., 2013; Shiozaki et al., 2014; Siefert et al., 1999). Dissolved iron concentrations measured during the WOCE IO5 and IO6 expeditions that sampled the Agulhas region were high, >1 nM at the shelf and >0.3 nM in the current, and attributed to the entrainment of sedimentary iron by the Agulhas Current, augmented by local iron deposition (Grand, Measures, Hatta, Morton, et al., 2015). Thus, the supply of both excess P and iron appear to be sufficient to support significant rates of N_2 fixation in Agulhas surface waters. Similar conditions likely fuel N_2 fixation elsewhere in the basin too, such as north and west of the Mascarene Plateau (i.e., 5–20°S, 50–60°E; Figure 5), and at the west Australian margin.

The nitrate isotopes indicate that N_2 fixation occurs predominantly in the greater Agulhas region of the subtropical gyre (as well as in the northern tropics and/or Mozambique Channel) and not in the more sluggish waters of the subtropical gyre's northern and eastern limbs (Sigman & Fripiat, 2019). This finding differs from N_2 fixation distributions diagnosed by models, which predict high rates in the southeast Indian basin (Deutsch et al., 2007; Wang et al., 2019). The overlap of excess P and iron across the Agulhas region may be enhanced by the retentive nature of the subtropical recirculation (Marshall et al., 2022), perhaps explaining why N_2 fixation occurs predominantly in the southwest Indian Ocean. Moreover, that the Agulhas Current entrains shelf-derived iron (Grand, Measures, Hatta, Morton, et al., 2015) and transports excess P waters into the greater Agulhas region suggests that the current plays a role in modulating both the rate and distribution of N_2 fixation in the southwest Indian Ocean. The Gulf Stream has similarly been shown to supply the adjacent subtropical North Atlantic with iron and excess P that sustain elevated N_2 fixation rates in the oligotrophic gyre waters (Conway et al., 2018; Palter et al., 2011).

4.3. Tracking Agulhas Leakage Using the Nitrate Isotopes

At the Agulhas Retroflection and in Agulhas eddies leaking into the Cape Basin, rapid heat loss (and thus evaporation) can erode the relatively fresh signal of surface to sub-thermocline Agulhas waters compared to those in the more saline South Atlantic (Gordon, 1987; D. Olson et al., 1992). During this modification, convective mixing may ventilate waters down to the 27.0 $kg.m^{-3}$ isopycnal (Gordon, 1987), which weakens upper water column gradients, thus limiting the utility of physical tracers (i.e., temperature and salinity) for identifying Agulhas leakage (D. Olson et al., 1992). However, nitrate Δ(15–18) is conserved during mixing (Rafter et al., 2013), such that it may be useful for tracking Agulhas leakage.

Agulhas leakage first enters the South Atlantic via the Cape Basin (Figure 1) where upper water column nitrate Δ(15–18) is relatively high (~2.9‰; squares in Figure 8) and indistinct from the underlying SAMW (Campbell, 2016; Flynn et al., 2020; Marconi et al., 2017). This high-Δ(15–18) nitrate derives from the complete consumption in subtropical surface waters of high-$\delta^{15}N$ nitrate that is laterally advected into the subtropical South Atlantic from the Southern Ocean (Campbell, 2016; Marconi et al., 2017). In addition, N_2 fixation, which lowers nitrate Δ(15–18), is thought to be negligible across the subtropical South Atlantic, unlike in the North Atlantic and North Pacific subtropical gyres (Fernández et al., 2010; Landolfi et al., 2018; Marconi et al., 2017; Moore et al., 2009; Shiozaki et al., 2017). In contrast to the South Atlantic, the Δ(15–18) of nitrate in the upper water column of the greater Agulhas region is low (mean of 1.6‰, with a minimum of −0.5‰) and should persist in Agulhas-derived waters transported into the South Atlantic. While assimilation by phytoplankton of Agulhas thermocline nitrate in Agulhas leakage will raise its $\delta^{15}N$, it will raise its $\delta^{18}O$ to the same extent (J. Granger et al., 2004, 2010), leaving the characteristic Δ(15–18) of Agulhas nitrate unchanged. At the same time, mixing of Agulhas and South Atlantic waters at the retroflection will combine low- and high-Δ(15–18) nitrate, yielding

a Δ(15–18) for nitrate in Agulhas leakage that is lower than that of the South Atlantic and higher than that of the greater Agulhas region. Continuous mixing (i.e., entrainment and detrainment) with the surrounding Cape Basin waters may further alter the Agulhas nitrate pool. However, given the retentive (and downwelling) nature of Agulhas leakage features (Arhan et al., 2011; Fine et al., 1988; Gordon, 1987; Wallschuss et al., 2022), mixing will not fully erase the low-Δ(15–18) of Agulhas nitrate in Agulhas rings and eddies (Figure S10 in Supporting Information S1). As such, Agulhas leakage should retain a nitrate Δ(15–18) that is considerably lower than that of the Cape Basin.

Four nitrate isotope data sets from across the Cape Basin have sampled Agulhas leakage (see Figure 1 for sampling locations and Figure 8 for data (Campbell, 2016; R. Granger et al., 2023; Marconi et al., 2017; Smart et al., 2015; Smart et al., 2020)). Low nitrate Δ(15–18) is observed in the thermocline and mixed layer of these features (mean Δ(15–18) of 2.5 ± 0.6‰ for σ_θ < 26.4 kg.m^{-3} and 1.8 ± 0.8‰ for the mixed layer, with values as low as −0.7‰; diamonds outlined in green in Figure 8), in contrast to the background Cape Basin (mean Δ(15–18) of 2.9 ± 0.2‰ for σ_θ < 26.4 kg.m^{-3} and 2.7 ± 0.6‰ for the mixed layer; squares outlined in red in Figure 8). It is likely that Agulhas leakage perennially influences the mean state of the background Cape Basin since leakage features are constantly being eroded and incorporated into Cape Basin waters (Gordon, 2003; Wallschuss et al., 2022). Nevertheless, our observations of lower nitrate Δ(15–18) in Agulhas leakage support the hypothesis that this parameter retains the imprint of southwest Indian Ocean N cycle processes in the subtropical southeast Atlantic Ocean.

At the same time, the available Agulhas leakage data reveal little evidence of the low-δ^{15}N nitrate characteristic of Agulhas thermocline waters, except perhaps in the slightly lower δ^{15}N measured for similar nitrate concentrations in the leakage versus the background Cape Basin (compare diamonds outlined in green to squares outlined in red at ln([NO_3^-]) = 0.5–1.5 μM in Figure 8). Instead, the data show that subsurface nitrate δ^{15}N in Agulhas leakage is relatively high, typically >6.6‰ and never lower than 6.0‰ (squares in Figure 8; background Cape Basin thermocline nitrate-δ^{15}N averages 6.9‰). The absence of an N_2 fixation signal, as low-δ^{15}N thermocline nitrate, in Agulhas leakage can be explained by isotope fractionation during nitrate assimilation, which raises the δ^{15}N (and δ^{18}O) of nitrate. While the deep convective mixing characteristic of Agulhas rings and eddies will entrain low-δ^{15}N nitrate from the thermocline into the surface layer, its subsequent rapid consumption by phytoplankton will overprint its low δ^{15}N, but because of the equivalent assimilation-driven rise in nitrate δ^{18}O, will not erode its Δ(15–18).

Our findings highlight the potential utility of the dual isotopes of nitrate for tracking Agulhas leakage in the Cape Basin and across the South Atlantic. In the modern ocean, this tracer may be particularly useful for tracking older Agulhas eddies that can no longer be distinguished by sea level height anomalies, sea surface temperature, or salinity. Plankton fueled by nitrate ultimately supplied from the southwest Indian Ocean should preserve the low-δ^{15}N of Agulhas nitrate in their biomass even as this signal is eroded from the thermocline and surface nitrate pool by nitrate assimilation. The eventual sinking to the seafloor of some of these plankton (e.g., planktic foraminifera; single-celled zooplankton with calcite shells that include minute quantities of organic N, protecting it from isotopic alteration) may transfer the low-δ^{15}N of Agulhas nitrate to the sediment record (Martínez-García et al., 2014; Ren et al., 2009, 2012; Smart et al., 2018). Similarly, plankton fueled by nitrate ultimately sourced from the South Atlantic thermocline should impose a higher δ^{15}N on sedimenting material. The δ^{15}N of fossil foraminifera from the Cape Basin sediment record might thus be used to infer the strength of Agulhas leakage in the past.

5. Summary

This study provides the first biogeochemical characterization of the Agulhas Current and adjacent recirculating waters. We identify both Upper and Lower Circumpolar Deep Water in the Agulhas Current for the first time and distinguish between thermocline and sub-thermocline waters, often referred to collectively as central waters. These waters are fundamentally different from one another, both hydrographically (e.g., in salinity) and biogeochemically (e.g., in their nitrate concentration and isotopes). Both the tropical and subtropical thermocline waters in the greater Agulhas region bear the isotopic imprint of N_2 fixation, while underlying SAMW does not. From a one-box model that incorporates water volume, P, N, and N-isotope fluxes, we estimate a local N_2 fixation rate for the greater Agulhas region. While a lack of data from the South Indian Ocean introduces significant uncertainties that yield a wide range in the N_2 fixation rate estimates, we nonetheless calculate an N_2 fixation rate of between 7

and 25 Tg N.a^{-1}, the first observations-based estimate for the subtropical southwest Indian Ocean; consideration of various factors causes us to favor the lower portion of this range. Furthermore, the nitrate N and O isotopes indicate that nitrate assimilation is the dominant N cycle process occurring in the mixed layer of the Agulhas Current and adjacent recirculating waters, with nitrification confined to the subsurface. The implication of this finding is that export production in the greater Agulhas region can be estimated from the rate of nitrate assimilation plus N_2 fixation, with no need to account for nitrate regenerated in the mixed layer. Along with coupled partial nitrate assimilation and nitrification that occurs largely at the base of the mixed layer, N_2 fixation generates low Δ(15–18) nitrate in the Agulhas thermocline and mixed layer. As such, we propose that Agulhas leakage into the South Atlantic can be tracked using nitrate Δ(15–18) even as the low-δ^{15}N of Agulhas thermocline nitrate is eroded by isotopic fractionation during in situ nitrate assimilation by phytoplankton. This result may have implications for using the N isotopes in the Cape Basin sediment record to reconstruct past Agulhas leakage.

Data Availability Statement

Data from the ASCA16, IIEO2, SWINGS, and ASCA summer 2018 cruises can be found in the Zenodo database (https://doi.org/10.5281/zenodo.7628608). Nitrate isotope data collected during the SAMBA 2015 and 2017 cruises are published Marconi et al. (2017) and R. Granger et al. (2023) and can also be found in the Zenodo database (https://doi.org/10.5281/zenodo.7648606).

Acknowledgments

We thank the captain and crew of the R/V *SA Agulhas II* and R/V *Marion Dufresne*, and the ASCA16, IIOE2, and SWINGS cruise enablers and participants, particularly Isabelle Ansorge, Raquel Flynn, Tahlia Henry, Ashley Johnson, Tamaryn Morris, Keshnee Pillay, and David Walker. We are particularly grateful to Heather Forrer and Thomas Ryan-Keogh for sample collection during the SWINGS cruise. We are also grateful to Olivier Crispi, Barbara Hinnenberg, Mareike Schmitt, and Florian Rubach for help with sample analysis. This research was supported by the South African National Research Foundation (114673 and 130826 to T.M., 115335, 129320, and 116142 to S.F.), the University of Cape Town (T.M., S.F., and K.S.), and the Royal Society and African Academy of Sciences (FLAIR fellowship to S.F.). The authors also acknowledge the support of the South African Department of Forestry, Fisheries, and the Environment and the Department of Science and Innovation's Biogeochemistry Research Infrastructure Platform (BIOGRIP), as well as the Max Planck Society, the Werner Siemens Foundation (S/Y Eugen Seibold founding agreement to G.H.H.) and United States National Science Foundation (1459543; the Agulhas System Climate Array to L.M.B.; 1851430 to D.M.S.).

References

Altabet, M. (1988). Variations in nitrogen isotopic composition between sinking and suspended particles: Implications for nitrogen cycling and particle transformation in the open ocean. *Deep-Sea Research*, *35*(4), 535–554. https://doi.org/10.1016/0198-0149(88)90130-6

Altieri, K., Fawcett, S., & Hastings, M. (2021). Reactive nitrogen cycling in the atmosphere and ocean. *Annual Review of Earth and Planetary Sciences*.

Argo. (2021). *Argo float data and metadata from Global Data Assembly Centre (Argo GDAC)*. SEANOE. https://doi.org/10.17882/42182

Arhan, M., Speich, S., Messager, C., Dencausse, G., Fine, R., & Boye, M. (2011). Anticyclonic and cyclonic eddies of subtropical origin in the subantarctic zone south of Africa. *Journal of Geophysical Research*, *116*(C11), C11004. https://doi.org/10.1029/2011JC007140

Armbrecht, L., Schaeffer, A., Roughan, M., & Armand, L. (2015). Interactions between seasonality and oceanic forcing drive the phytoplankton variability in the tropical-temperate transition zone (~30°S) of eastern Australia. *Journal of Marine Systems*, *144*, 92–106. https://doi.org/10.1016/j.jmarsys.2014.11.008

Baker, A., Lesworth, T., Adams, C., Jickells, T. D., & Ganzeveld, L. (2010). Estimation of atmospheric nutrient inputs to the Atlantic Ocean from 50°N to 50°S based on large-scale field sampling: Fixed nitrogen and dry deposition of phosphorus. *Global Biogeochemical Cycles*, *24*(3), https://doi.org/10.1029/2009gb003634

Bang, N. (1970). Dynamic interpretations of a detailed surface temperature chart of the Agulhas Current retroflexion (sic) and fragmentation area. *Journal of South African Geography*, *52*(1), 67–76. https://doi.org/10.1080/03736245.1970.10559466

Bange, H., Rixen, T., Johansen, A., Siefert, R., Ramesh, R., Ittekkot, V., et al. (2000). First direct measurements of N_2 fixation during a *Trichodesmium* bloom in the eastern Arabian Sea. *Global Biogeochemical Cycles*, *14*(4), 1283–1297. https://doi.org/10.1029/1999gb001228

Beal, L., Chereskin, T., Lenn, Y., & Elipot, S. (2006). The sources and mixing characteristics of the Agulhas Current. *Journal of Physical Oceanography*, *36*(11), 2060–2074. https://doi.org/10.1175/jpo2964.1

Beal, L., De Ruijter, W. P. M., Biastoch, A., Zahn, R., Cronin, M., Hermes, J., et al. (2011). On the role of the Agulhas system in ocean circulation and climate. *Nature Review*, *472*(7344), 429–436. https://doi.org/10.1038/nature09983

Beal, L., Elipot, S., Houk, A., & Leber, G. (2015). Capturing the transport variability of a western boundary jet: Results from the Agulhas Current time-series experiment (ACT). *Journal of Physical Oceanography*, *45*(5), 1302–1324. https://doi.org/10.1175/JPO-D-14-0119.1

Beal, L., Ffield, A., & Gordon, A. (2000). Spreading of Red Sea overflow waters in the Indian Ocean. *Journal of Geophysical Research*, *105*(C4), 8549–8564. https://doi.org/10.1029/1999JC900306C

Bianchi, D., Dunne, J., Sarmiento, J., & Galbraith, E. (2012). Data-based estimates of suboxia, denitrification, and N_2O production in the ocean and their sensitivities to dissolved O_2. *Global Biogeochemical Cycles*, *26*(GB2009). https://doi.org/10.1029/2011GB004209

Blain, S., Capparos, J., Gueneugues, A., Obernosterer, I., & Oriol, L. (2015). Distributions and stoichiometry of dissolved nitrogen and phosphorus in the iron-fertilized region near Kerguelen (Southern Ocean). *Biogeosciences*, *12*(2), 623–635. https://doi.org/10.5194/bg-12-623-2015

Böhlke, J., Mroczkowski, S. J., & Coplen, T. (2003). Oxygen isotopes in nitrate: New reference materials for 18O:17O:16O measurements and observations on nitrate-water equilibration. *Rapid Communications in Mass Spectrometry*, *17*(16), 1835–1846. https://doi.org/10.1002/rcm.1123

Boshers, D., Granger, J., Tobias, C. R., Bohlke, J. K., & Smith, R. L. (2019). Constraining the oxygen isotopic composition of nitrate produced by nitrification. *Environmental Science and Technology*, *53*(3), 1206–1216. https://doi.org/10.1021/acs.est.8b03386

Bower, A. (1991). A simple kinematic mechanism for mixing fluid parcels across a meandering jet. *Journal of Physical Oceanography*, *21*(1), 173–180. https://doi.org/10.1175/1520-0485(1991)021<0173:askmfm>2.0.co;2

Bower, A., Hunt, H., & Price, J. (2000). Character and dynamics of the Red Sea and Persian Gulf outflows. *Journal of Geophysical Research*, *105*(C3), 6387–6414. https://doi.org/10.1029/1999JC900297

Bower, A., Rossby, H., & Lillibridge, J. (1985). The Gulf Stream- barrier or blender? *Journal of Physical Oceanography*, *15*(1), 24–32. https://doi.org/10.1175/1520-0485(1985)015<0024:tgsob>2.0.co;2

Brandes, J., Devol, A. H., Yoshinari, T., Jayakumar, D. A., & Naqvi, S. W. A. (1998). Isotopic composition of nitrate in the central Arabian Sea and eastern tropical North Pacific: A tracer for mixing and nitrogen cycles. *Limnology & Oceanography*, *43*(7), 1680–1689. https://doi.org/10.4319/lo.1998.43.7.1680

Bryden, H., & Beal, L. (2001). Role of the Agulhas Current in Indian Ocean circulation and associated heat and freshwater fluxes. *Deep-Sea Research*, *48*(8), 1821–1845. https://doi.org/10.1016/s0967-0637(00)00111-4

Bryden, H., Beal, L., & Duncan, L. (2005). Structure and transport of the Agulhas Current and its temporal variability. *Journal of Oceanography*, *61*(3), 479–492. https://doi.org/10.1007/s10872-005-0057-8

Buchwald, C., Santoro, A., McIlvin, M., & Casciotti, K. (2012). Oxygen isotopic composition of nitrate and nitrite produced by nitrifying cocultures and natural marine assemblages. *Limnology & Oceanography*, *57*(5), 1361–1375. https://doi.org/10.4319/lo.2012.57.5.1361

Campbell, E. (2016). Where three oceans meet: Nitrate isotope measurements from the South Atlantic along 34.5S. Senior thesis. Princeton University.

Capone, D., Subramaniam, A., Montoya, J., Voss, M., Humborg, C., Johansen, A., et al. (1998). An extensive bloom of the N_2-fixing cyanobacterium Trichodesmium erythraeum in the central Arabian Sea. *Marine Ecology Progress Series*, *172*, 281–292. https://doi.org/10.3354/meps172281

Carpenter, E., Harvey, H., Fry, B., & Capone, D. G. (1997). Biogeochemical tracers of the marine cyanobacterium Trichodesmium. *Deep Sea Research I*, *44*(1), 27–38. https://doi.org/10.1016/s0967-0637(96)00091-x

Casciotti, K., & McIlvin, M. (2007). Isotopic analyses of nitrate and nitrite from reference mixtures and application to eastern tropical North Pacific waters. *Marine Chemistry*, *107*(2), 184–201. https://doi.org/10.1016/j.marchem.2007.06.021

Casciotti, K., McIlvin, M., & Buchwald, C. (2010). Oxygen isotopic exchange and fractionation during bacterial ammonia oxidation. *Limnology & Oceanography*, *55*(2), 753–762. https://doi.org/10.4319/lo.2010.55.2.0753

Casciotti, K., Sigman, D. M., Hastings, M. G., Bohlke, J. K., & Hilkert, A. (2002). Measurement of the oxygen isotopic composition of nitrate in seawater and freshwater using the denitrifier method. *Analytical Chemistry*, *74*(19), 4905–4912. https://doi.org/10.1021/ac020113w

Cerdan-Garcia, E., Baylay, A., Polyviou, D., Woodward, E. M. S., Wrightson, L., Mahaffey, C., et al. (2022). Transcriptional responses of Trichodesmium to natural inverse gradients of Fe and P availability. *The ISME Journal*, *16*(4), 1055–1064. https://doi.org/10.1038/s41396-021-01151-1

Chinni, V., & Singh, S. (2022). Dissolved iron cycling in the Arabian Sea and sub-tropical gyre region of the Indian Ocean. *Geochimica et Cosmochimica Acta*, *317*, 325–348. https://doi.org/10.1016/j.gca.2021.10.026

Conway, T., Palter, J., & Souza, G. D. (2018). Gulf Stream rings as a source of iron to the North Atlantic subtropical gyre. *Nature Geoscience*, *11*(8), 594–598. https://doi.org/10.1038/s41561-018-0162-0

Copin-Montegut, C., & Copin-Montegut, G. (1978). The chemistry of particulate matter from the South Indian and Antarctic oceans. *Deep Sea Research*, *25*(10), 911–931. https://doi.org/10.1016/0146-6291(78)90633-1

Cronin, M. F., Bond, N., Booth, J., Ichikawa, H., Joyce, T. M., Kelly, K., et al. (2010). Monitoring ocean-atmosphere interactions in western boundary current extensions. In *OceanObs'09 Conference Proceeding*.

Deman, F., Fonseca-Batista, D., Roukaerts, A., Garcia-Ibanez, M. I., Le Roy, E., Thilakarathne, E. P. D. N., et al. (2021). Nitrate supply routes and impact of internal cycling in the North Atlantic Ocean inferred from nitrate isotopic composition. *Global Biogeochemical Cycles*, *35*(4). https://doi.org/10.1029/2020GB006887

de Ruijter, W., Biastoch, A., Drijfhout, S. S., Lutjeharms, J. R. E., Matano, R. P., Pichevin, T., et al. (1999). Indian-Atlantic interocean exchange: Dynamics, estimation and impact. *Journal of Geophysical Research*, *104*(C9), 20885–20910. https://doi.org/10.1029/1998jc900099

Detoni, A. M. S., Ciotti, A. M., Calil, P. H. R., Tavano, V. M., & Yunes, J. S. (2016). Trichodesmium latitudinal distribution on the shelf break in the southwestern Atlantic Ocean during spring and autumn. *Global Biogeochemical Cycles*, *30*(11), 1738–1753. https://doi.org/10.1002/2016GB005431

Deutsch, C., Sarmiento, J. L., Sigman, D. M., Gruber, N., & Dunne, J. P. (2007). Spatial coupling of nitrogen inputs and losses in the ocean. *Nature Articles*, *445*(7124), 163–167. https://doi.org/10.1038/nature05392

DeVries, T., Deutsch, C., Rafter, P., & Primeau, F. (2013). Marine denitrification rates determined from a global 3-D inverse model. *Biogeosciences*, *10*(4), 2481–2496. https://doi.org/10.5194/bg-10-2481-2013

Diamond, D. (1994). *QuikChem Method 10-114-21-1-B: Silicate by flow injection analysis*, s.l.: Lachat Instruments.

DiFiore, P., Sigman, D., & Dunbar, R. (2009). Upper ocean nitrogen fluxes in the Polar Antarctic Zone: Constraints from the nitrogen and oxygen isotopes of nitrate. *Geochemistry, Geophysics, Geosystems*, *10*(11), Q11016. https://doi.org/10.1029/2009GC002468

DiFiore, P., Sigman, D. M., Trull, T. W., Lourey, M. J., Karsh, K., Cane, G., & Ho, R. (2006). Nitrogen isotope constraints on subantarctic biogeochemistry. *Journal of Geophysical Research*, *111*(C08016), C08016. https://doi.org/10.1029/2005JC003216

DiMarco, S., Chapman, P., Nowlin, W. D., Hacker, P., Donohue, K., Luther, M., et al. (2002). Volume transport and property distributions of the Mozambique Channel. *Deep-Sea Research II*, *49*(7–8), 1481–1511. https://doi.org/10.1016/s0967-0645(01)00159-x

Donohue, K., & Toole, J. (2003). A near-synoptic survey of the Southwest Indian Ocean. *Deep-Sea Research II*, *50*(12–13), 1893–1931. https://doi.org/10.1016/s0967-0645(03)00039-0

Ducet, N., Le Traon, P., & Reverdin, G. (2000). Global high-resolution mapping of ocean circulation from TOPEX/Poseidon and ERS-1 and -2. *Journal of Geophysical Research*, *105*(C8), 19477–19498. https://doi.org/10.1029/2000jc900063

Dugdale, R., & Goering, J. (1967). Uptake of new and regenerated forms of nitrogen in primary productivity. *Limnology & Oceanography*, *12*(2), 196–206. https://doi.org/10.4319/lo.1967.12.2.0196

Emerson, S. (2014). Annual net community production and the biological carbon flux in the ocean. *Global Biogeochemical Cycles*, *28*(1), 14–28. https://doi.org/10.1002/2013GB004680

Eppley, R., & Peterson, B. (1979). Particulate organic matter flux and planktonic new production in the deep ocean. *Nature Articles*, *282*(5740), 677–680. https://doi.org/10.1038/282677a0

Fawcett, S., Johnson, K. S., Riser, S. C., Van Oostende, N., & Sigman, D. M. (2018). Low-nutrient organic matter in the Sargasso Sea thermocline: A hypothesis for its role, identity, and carbon cycle implications. *Marine Chemistry*, *207*, 108–123. https://doi.org/10.1016/j.marchem.2018.10.008

Fawcett, S., Lomas, M. W., Casey, J. R., Ward, B. B., & Sigman, D. M. (2011). Assimilation of upwelled nitrate by small eukaryotes in the Sargasso Sea. *Nature Geoscience*, *4*(10), 717–722. https://doi.org/10.1038/NGEO1265

Fawcett, S., Ward, B., Lomas, M., & Sigman, D. (2015). Vertical decoupling of nitrate assimilation and nitrification in the Sargasso Sea. *Deep-Sea Research I*, *103*, 64–72. https://doi.org/10.1016/j.dsr.2015.05.004

Fernández, A., Mourino-Carballido, B., Bode, A., Varela, M., & Maranon, E. (2010). Latitudinal distribution of trichodesmium spp. and N_2 fixation in the Atlantic Ocean. *Biogeosciences*, *7*(10), 3167–3176. https://doi.org/10.5194/bg-7-3167-2010

Fine, R. (1993). Circulation of Antarctic intermediate water in the South Indian Ocean. *Deep-Sea Research I*, *40*(10), 2021–2042. https://doi.org/10.1016/0967-0637(93)90043-3

Fine, R., Smethie, W. M., Bullister, J. L., Rhein, M., Min, D. H., Warner, M. J., et al. (2008). Decadal ventilation and mixing of Indian Ocean waters. *Deep-Sea Research Part I*, *55*(1), 20–37. https://doi.org/10.1016/j.dsr.2007.10.002

Fine, R., Warner, M., & Weiss, R. (1988). Water mass modification at the Agulhas retroflection: Chlorofluoromethane studies. *Deep-Sea Research*, *35*(3), 311–332. https://doi.org/10.1016/0198-0149(88)90013-1

Flynn, R., Granger, J., Veitch, J. A., Siedlecki, S., Burger, J. M., Pillay, K., & Fawcett, S. E. (2020). On-shelf nutrient trapping enhances the fertility of the southern Benguela upwelling system. *Journal of Geophysical Research: Oceans*, *125*(6), e2019JC015948. https://doi.org/10.1029/2019JC015948

Fripiat, F., Martinez-Garcia, A., Fawcett, S. E., Kemeny, P. C., Studer, A. S., Smart, S. M., et al. (2019). The isotope effect of nitrate assimilation in the Antarctic Zone: Improved estimates and paleoceanographic implications. *Geochimica et Cosmochimica Acta*, *247*, 261–279. https://doi.org/10.1016/j.gca.2018.12.003

Fripiat, F., Martinez-Garcia, A., Marconi, D., Fawcett, S. E., Kopf, S. H., Luu, V. H., et al. (2021). Nitrogen isotopic constraints on nutrient transport to the upper ocean. *Nature Geoscience*, *14*(11), 855–861. https://doi.org/10.1038/s41561-021-00836-8

Gandhi, N., Singh, A., Prakash, S., Ramesh, R., Raman, M., Sheshshayee, M. S., & Shetye, S. (2011). First direct measurements of N_2 fixation during a Trichodesmium bloom in the eastern Arabian Sea. *Global Biogeochemical Cycles*, *25*, GB4014. https://doi.org/10.1029/2010GB003970

Garcia, H. E., Weathers, K., Paver, C. R., Smolyar, I., Boyer, T. P., Locarnini, R. A., et al. (2018). World Ocean Atlas 2018, volume 4: Dissolved inorganic nutrients (phosphate, nitrate, nitrate+nitrite, silicate). A. Mishonov Technical Ed.; *Silver Spring: NOAA Atlas NESDIS*, *84*, 35.

Gaye, B., Nagel, B., Dahnke, K., Rixen, T., & Emeis, K. C. (2013). Evidence of parallel denitrification and nitrite oxidation in the ODZ of the Arabian Sea from paired stable isotopes of nitrate and nitrite. *Global Biogeochemical Cycles*, *27*(4), 1059–1071. https://doi.org/10.1002/2011gb004115

Gonfiantini, R. (1984). Stable isotope reference samples for geochemical and hydrological investigations. *The International Journal of Applied Radiation and Isotopes*, *35*(5), 426. https://doi.org/10.1016/0020-708X(84)90059-0

Gordon, A. (1985). Indian-Atlantic transfer of thermocline water at the Agulhas retroflection. *Science*, *277*(4690), 1030–1033. https://doi.org/10.1126/science.227.4690.1030

Gordon, A. (2003). The brawniest retroflection. *Nature*, *421*(6926), 904–905. https://doi.org/10.1038/421904a

Gordon, A., Lutjeharms, J. R., & Grundlingh, M. L. (1987). Stratification and circulation at the Agulhas Retroflection. *Deep-Sea Research*, *34*(4), 565–599. https://doi.org/10.1016/0198-0149(87)90006-9

Gordon, A., Ma, S., Olson, D. B., Hacker, P., Ffield, A., Talley, L. D., et al. (1997). Advection and diffusion of Indonesian throughflow water within the Indian Ocean south equatorial current. *Geophysical Research Letters*, *24*(21), 2573–2576. https://doi.org/10.1029/97GL01061

Grand, M., Measures, C. I., Hatta, M., Hiscock, W. T., Buck, C. S., & Landing, W. M. (2015). Dust deposition in the eastern Indian Ocean: The ocean perspective from Antarctica to the Bay of Bengal. *Global Biogeochemical Cycles*, *29*(3), 357–374. https://doi.org/10.1002/2014GB004898

Grand, M., Measures, C. I., Hatta, M., Morton, P. L., Barrett, P., Milne, A., et al. (2015). The impact of circulation and dust deposition in controlling the distributions of dissolved Fe and Al in the south Indian subtropical gyre. *Marine Chemistry*, *176*, 110–125. https://doi.org/10.1016/j.marchem.2015.08.002

Granger, J., & Sigman, D. (2009). Removal of nitrite with sulfamic acid for nitrate N and O isotope analysis with the denitrifier method. *Rapid Communications in Mass Spectrometry*, *23*, 3753–3762. https://doi.org/10.1002/rcm.4307

Granger, J., Sigman, D., Lehmann, M., & Tortell, P. (2008). Nitrogen and oxygen isotope fractionation during dissimilatory nitrate reduction by denitrifying bacteria. *Limnology & Oceanography*, *53*(6), 2533–2545. https://doi.org/10.4319/lo.2008.53.6.2533

Granger, J., Sigman, D., Needoba, J., & Harrison, P. (2004). Coupled nitrogen and oxygen isotope fractionation of nitrate during assimilation by cultures of marine phytoplankton. *Limnology & Oceanography*, *49*(5), 1763–1773. https://doi.org/10.4319/lo.2004.49.5.1763

Granger, J., Sigman, D., Rohde, M., Maldonado, M., & Tortell, P. (2010). N and O isotope effects during nitrate assimilation by unicellular prokaryotic and eukaryotic plankton cultures. *Geochimica et Cosmochimica Acta*, *74*(3), 1030–1040. https://doi.org/10.1016/j.gca.2009.10.044

Granger, R., Smart, S. M., Foreman, A., Auderset, A., Campbell, E. C., Marshall, T. A., et al. (2023). Southeast Atlantic nitrate isotope data from winter 2017 [Dataset]. Zenodo. https://doi.org/10.5281/zenodo.7648606

Grasshoff, K. (1976). *Methods of seawater analysis*. Verlag Chemie.

Grasshoff, K., Kremling, K., & Ehrhardt, M. (1999). Methods of seawater analysis, Third edition. In K. Grasshoff, K. Ehrhardt, & K. Kremling (Eds.), *Verlag chemie* (2nd ed., p. 419). Wiley-VCH.

Gruber, N., & Sarmiento, J. (1997). Global patterns of marine nitrogen fixation and denitrification. *Global Biogeochemical Cycles*, *11*(2), 235–266. https://doi.org/10.1029/97gb00077

Gründlingh, M., Carter, R., & Stanton, R. (1991). Circulation and water properties of the southwest Indian Ocean. *Progress in Oceanography*, *28*(4), 305–342. https://doi.org/10.1016/0079-6611(91)90031-g

Gunn, K. L., Beal, L. M., Elipot, S., McMonigal, K., & Houk, A. (2020). Mixing of subtropical, central, and intermediate waters driven by shifting and pulsing of the Agulhas current. *Journal of Physical Oceanography*, *50*(12), 3545–3560. https://doi.org/10.1175/JPO-D-20-0093.1

Guo, X., Zhu, X., Wu, Q., & Huang, D. (2012). The Kuroshio nutrient stream and its temporal variation in the East China Sea. *Journal of Geophysical Research*, *117*, C01026. https://doi.org/10.1029/2011JC007292

Harms, N., Lahajnar, N., Gaye, B., Rixen, T., Dahnke, K., Ankele, M., et al. (2019). Nutrient distribution and nitrogen and oxygen isotopic composition of nitrate in water masses of the subtropical South Indian Ocean. *Biogeosciences*. https://doi.org/10.5194/bg-2018-511

Held, M., Webb, E. A., McIlvin, M. M., Hutchins, D. A., Cohen, N. R., Moran, D. M., et al. (2020). Co-occurrence of Fe and P stress in natural populations of the marine diazotroph Trichodesmium. *Biogeosciences*, *17*(9), 2537–2551. https://doi.org/10.5194/bg-17-2537-2020

Herraiz-Borreguero, L., & Rintoul, S. (2011). Subantarctic mode water: Distribution and circulation. *Ocean Dynamics*, *61*(1), 103–126. https://doi.org/10.1007/s10236-010-0352-9

Hoering, T., & Ford, H. (1960). The isotope effect in the fixation of nitrogen by Azotobacter. *Journal of the American Chemical Society*, *82*(2), 376–378. https://doi.org/10.1021/ja01487a031

Howe, P., Donohue, K., & Watts, D. (2009). Stream-coordinate structure and variability of the Kuroshio extension. *Deep Sea Research Part I: Oceanographic Research Papers*, *56*(7), 1093–1116. https://doi.org/10.1016/j.dsr.2009.03.007

Huggett, J., & Kyewalyanga, M. (2017). Chapter 5: Ocean productivity. In J. Groeneveld, & K. Koranteng (Eds.), *The RV Dr Fridtjof Nansen in the western Indian Ocean: Voyages of marine research and capacity development* (Vol. 55, p. 80). FAO.

Imawaki, S., Bower, A., Beal, L., & Qui, B. (2013). Chapter 13- western boundary currents. In G. Siedler, S. Griffies, J. Gould, & J. Church (Eds.), *Ocean circulation and climate: A 21st century perspective*. (pp. 305–338). s.l: International Geophysics.

Jickells, T., Buitenhuis, E., Altieri, K., Baker, A. R., Capone, D., Duce, R. A., et al. (2017). A re-evaluation of the magnitude and impacts of anthropogenic atmospheric nitrogen inputs on the ocean: Duce et al revisited. *Global Biogeochemical Cycles*, *31*. https://doi.org/10.1002/2016GB005586

Karlusich, J., Pelletier, E., Lombard, F., Carsique, M., Dvorak, E., Colin, S., et al. (2021). Global distribution patterns of marine nitrogen fixers by imaging and molecular methods. *Nature Communications*, *12*(4160), 4160. https://doi.org/10.1038/s41467-021-24299-y

Karstensen, J., & Tomczak, M. (1997). Ventilation processes and water mass ages in the thermocline of the southeast Indian Ocean. *Journal od Geophysical Research*, *24*(22), 2777–2780. https://doi.org/10.1029/97gl02708

Kemeny, P., Weigand, M. A., Zhang, R., Carter, B. R., Karsh, K. L., Fawcett, S. E., & Sigman, D. M. (2016). Enzyme-level interconversion of nitrate and nitrite in the fall mixed layer of the Antarctic Ocean. *Global Biogeochemical Cycles*, *30*(7), 1069–1085. https://doi.org/10.1002/2015GB005350

Kirk, J. (1994). *Light and photosynthesis in aquatic ecosystems*. 2nd ed. s.l.: Cambridge University Press.

Klawonn, I., Lavik, G., Boning, P., Marchant, H. K., Dekaezemacker, J., Mohr, W., & Ploug, H. (2015). Simple approach for the preparation of $^{15-15}N_2$-enriched water for nitrogen fixation assessments: Evaluation, application and recommendations. *Fontiers in Microbiology*, *6*(769). https://doi.org/10.3389/fmicb.2015.00769

Knapp, A., DiFiore, P., Deutsch, C., Sigman, D., & Lipschultz, F. (2008). Nitrate isotopic composition between Bermuda and Puerto Rico: Implications for N_2 fixation in the Atlantic Ocean. *Global Biogeochemical Cycles*, *22*(3). https://doi.org/10.1029/2007gb003107

Knapp, A., McCabe, K. M., Grosso, O., Leblond, N., Moutin, T., & Bonnet, S. (2018). Distribution and rates of nitrogen fixation in the western tropical South Pacific Ocean constrained by nitrogen isotope budgets. *Biogeosciences*, *15*(9), 2619–2628. https://doi.org/10.5194/bg-15-2619-2018

Knapp, A., Sigman, D., & Lipschultz, F. (2005). N isotopic composition of dissolved organic nitrogen and nitrate at the Bermuda Atlantic Time-series Study site. *Global Biogeochemical Cycles*, *19*(1), https://doi.org/10.1029/2004gb002320

Knapp, A., Sigman, D. M., Lipschultz, F., Kustka, A. B., & Capone, D. G. (2011). Interbasin isotopic correspondence between upper-ocean bulk DON and subsurface nitrate and its implications for marine nitrogen cycling. *Global Biogeochemical Cycles*, *25*, GB4044. https://doi.org/10.1029/2010GB003878

Koch-Larrouy, A., Morrow, R., Penduff, T., & Juza, M. (2010). Origin and mechanism of subantarctic mode water formation and transformation in the southern Indian Ocean. *Ocean Dynamics*, *60*(3), 563–583. https://doi.org/10.1007/s10236-010-0276-4

Krug, M., Swart, S., & Gula, J. (2017). Submesoscale cyclones in the Agulhas Current. *Geophysical Research Letters*, *44*(1), 346–354. https://doi.org/10.1002/2016GL071006

Landolfi, A., Kähler, P., Koeve, W., & Oschlies, A. (2018). Global marine N_2 fixation estimates: From observations to models. *Frontiers in Microbiology: Mini review*, *9*. https://doi.org/10.3389/fmicb.2018.02112

Leber, G., & Beal, L. (2015). Local water mass modifications by a solitary meander in the Agulhas Current. *Journal of Geophysical Research: Oceans*, *120*(6), 4503–4515. https://doi.org/10.1002/2015jc010863

Leber, G., Beal, L., & Elipot, S. (2017). Wind and current forcing combine to drive strong upwelling in the Agulhas Current. *Journal of Physical Oceanography*, *47*(1), 123–134. https://doi.org/10.1175/jpo-d-16-0079.1

Lehmann, N., Granger, J., Kienast, M., Brown, K. S., Rafter, P. A., Martinez-Mendez, G., & Mohtadi, M. (2018). Isotopic evidence for the evolution of subsurface nitrate in the western equatorial Pacific. *Journal of Geophysical Research: Oceans*, *123*(3), 1684–1707. https://doi.org/10.1002/2017JC013527

Letscher, R., Hansell, D. A., Carlson, C. A., Lumpkin, R., & Knapp, A. N. (2013). Dissolved organic nitrogen in the global surface ocean: Distribution and fate. *Global Biogeochemical Cycles*, *27*(1), 141–153. https://doi.org/10.1029/2012gb004449

Lévy, M., Ferrari, R., Franks, P. J. S., Martin, A. P., & Riviere, P. (2012). Bringing physics to life at the submesoscale. *Geophysical Research Letters*, *39*, L14602. https://doi.org/10.1029/2012GL052756

Liang, Z., McCabe, K., Fawcett, S. E., Forrer, H. J., Hashihama, F., Jeandel, C., et al. (2022). A global ocean dissolved organic phosphorus concentration database (DOPv2021). *Nature Scientific Data*, *9*(1), 772. https://doi.org/10.1038/s41597-022-01873-7

Lomas, M., Bates, N., Johnson, R., Knap, A., Steinberg, D., & Carlson, C. (2013). Two decades and counting: 24-years of sustained open ocean biogeochemical measurements in the Sargasso Sea. *Deep-Sea Research II*, *93*, 16–32. https://doi.org/10.1016/j.dsr2.2013.01.008

Lu, Y., Liu, Q., & Xie, S. (2021). Covariability of subantarctic mode water and the southern branch of the subtropical Indian Ocean countercurrent in Argo observations. *Journal of Ocean University of China*, *20*(6), 1316–1324. https://doi.org/10.1007/s11802-021-4677-4

Lutjeharms, J. (1980). Retroflection; when the current turns. *Oceans*, *13*(31).

Lutjeharms, J., & Ansorge, I. (2001). The Agulhas return current. *Journal of Marine Systems*, *30*(1–2), 115–138. https://doi.org/10.1016/s0924-7963(01)00041-0

Marconi, D., Alexandra Weigand, M., Rafter, P. A., McIlvin, M. R., Forbes, M., Casciotti, K. L., & Sigman, D. M. (2015). Nitrate isotope distributions on the US GEOTRACES North Atlantic cross-basin section: Signals of polar nitrate sources and low latitude nitrogen cycling. *Marine Chemistry*, *177*(1), 143–156. https://doi.org/10.1016/j.marchem.2015.06.007

Marconi, D., Sigman, D. M., Casciotti, K. L., Campbell, E. C., Alexandra Weigand, M., Fawcett, S. E., et al. (2017). Tropical dominance of N_2 fixation in the North Atlantic Ocean. *Global Biogeochemical Cycles*, *31*(10), 1608–1623. https://doi.org/10.1002/2016gb005613

Marconi, D., Weigand, M., & Sigman, D. (2019). Nitrate isotopic gradients in the North Atlantic Ocean and the nitrogen isotopic composition of sinking organic matter. *Deep-Sea Research Part I*, *145*, 109–124. https://doi.org/10.1016/j.dsr.2019.01.010

Marshall, T., Granger, J., Casciotti, K. L., Dahnke, K., Emeis, K. C., Marconi, D., et al. (2022). The angola gyre is a hotspot of dinitrogen fixation in the South Atlantic Ocean. *Nature Communications Earth & Environment*, *3*(151), 151. https://doi.org/10.1038/s43247-022-00474-x

Martin, T., & Casciotti, K. (2017). Paired N and O isotopic analysis of nitrate and nitrite in the Arabian Sea oxygen deficient zone. *Deep-Sea Research I*, *121*, 121–131. https://doi.org/10.1016/j.dsr.2017.01.002

Martínez-García, A., Sigman, D. M., Ren, H., Anderson, R. F., Straub, M., Hodell, D. A., et al. (2014). Iron fertilization of the Subantarctic ocean during the last ice age. *Science*, *343*(6177), 1347–1350. https://doi.org/10.1126/science.1246848

Martiny, A., Pham, C. T. A., Primeau, F. W., Vrugt, J. A., Moore, J. K., Levin, S. A., & Lomas, M. W. (2013). Strong latitudinal patterns in the elemental ratios of marine plankton and organic matter. *Nature Geoscience Letters*, *6*(4), 279–283. https://doi.org/10.1038/ngeo1757

McCartney, M. (1982). The subtropical recirculation of mode waters. *Journal of Marine Research*, *40*(Supplement), 427–464.

McDonagh, E., Bryden, H. L., King, B. A., Sanders, R. J., Cunningham, S. A., & Marsh, R. (2005). Decadal changes in the South Indian Ocean Thermocline. *Journal of Climate*, *18*(10), 1575–1590. https://doi.org/10.1175/jcli3350.1

McMonigal, K., Beal, L. M., Elipot, S., Gunn, K. L., Hermes, J., Morris, T., & Houk, A. (2020). The impact of meanders, deepening and broadening, and seasonality on Agulhas Current temperature variability. *Journal of Physical Oceanography*, *50*(12), 3529–3544. https://doi.org/10.1175/JPO-D-20-0018.1

Mdutyana, M., Thomalla, S. J., Philibert, R., Ward, B. B., & Fawcett, S. E. (2020). The seasonal cycle of nitrogen uptake and nitrification in the Atlantic sector of the Southern Ocean. *Global Biogeochemical Cycles*, *34*(7). https://doi.org/10.1029/2019GB006363

Merbt, S., Stahl, D. A., Casamayor, E. O., Marti, E., Nicol, G. W., & Prosser, J. I. (2012). Differential photoinhibition of bacterial and archaeal ammonia oxidation. *FEMS Microbiology Letters*, *327*(1), 41–46. https://doi.org/10.1111/j.1574-6968.2011.02457.x

Metzl, N., Lo Monaco, C., Leseurre, C., Ridame, C., Fin, J., Mignon, C., et al. (2022). The impact of the South-East Madagascar Bloom on the oceanic CO_2 sink. *Biogeosciences*, *19*(5), 1451–1468. https://doi.org/10.5194/bg-19-1451-2022

Mills, M., Ridame, C., Davey, M., La Roche, J., & Geider, R. J. (2004). Iron and phosphorus co-limit nitrogen fixation in the eastern tropical North Atlantic. *Nature Letters*, *429*(6989), 292–294. https://doi.org/10.1038/nature02550

Minagawa, M., & Wada, E. (1986). Nitrogen isotope ratios of red tides organisms in the East China Sea: A characterisation of biological nitrogen fixation. *Marine Chemistry*, *19*(3), 245–259. https://doi.org/10.1016/0304-4203(86)90026-5

Mohr, W., Grosskopf, T., Wallace, D., & LaRoche, J. (2010). Methodological underestimation of oceanic nitrogen fixation rates. *PLoS One*, *8*(9), e12583. https://doi.org/10.1371/journal.pone.0012583

Montoya, J., Voss, M., Kahler, P., & Capone, D., (1996). A simple, high-precision, high-sensitivity tracer assay for N_2 fixation. *Application of Environmental Microbiology*, *62*(3), 986–993. https://doi.org/10.1128/AEM.62.3.986-993.1996

Moore, C., Mills, M. M., Achterberg, E. P., Geider, R. J., LaRoche, J., Lucas, M. I., et al. (2009). Large-scale distribution of Atlantic nitrogen fixation controlled by iron availability. *Nature Geoscience*, *2*(12), 867–871. https://doi.org/10.1038/ngeo667

Nishioka, J., Obata, H., & Tsumune, D. (2013). Evidence of an extensive spread of hydrothermal dissolved iron in the Indian Ocean. *Earth and Planetary Science Letters*, *361*, 26–33. https://doi.org/10.1016/j.epsl.2012.11.040

Okin, G. S., Baker, A. R., Tegen, I., Mahowald, N. M., Dentener, F. J., Duce, R. A., et al. (2011). Impacts of atmospheric nutrient deposition on marine productivity: Roles of nitrogen, phosphorus, and iron. *Global Biogeochemical Cycles*, *25*, GB2022. https://doi.org/10.1029/2010GB003858

Olson, D., Fine, R., & Gordon, A. (1992). Convective modifications of water masses in the Agulhas. *Deep-Sea Research*, *39*, S163–S181. https://doi.org/10.1016/S0198-0149(11)80010-5

Olson, R. (1981). Differential photoinhibition of marine nitrifying bacteria: A possible mechanism for the formation of the primary nitrite maximum. *Journal of Marine Research*, *39*, 227–238.

Palter, J. B., Lozier, M., & Barber, R. (2005). The effect of advection on the nutrient reservoir in the North Atlantic subtropical gyre. *Nature*, *437*(29), 687–692. https://doi.org/10.1038/nature03969

Palter, J. B., Lozier, S., Sarmiento, J., & Williams, R. (2011). The supply of excess phosphate across the Gulf Stream and the maintenance of subtropical nitrogen fixation. *Global Biogeochemical Cycles*, *25*, GB4007. https://doi.org/10.1029/2010GB003955

Palter, J. B., Marinov, I., Sarmiento, J., & Gruber, N. (2013). Large-scale, persistent nutrient fronts of the world ocean: Impacts on biogeochemistry. In I. Belkim (Ed.), *Chemical oceanography of frontal zones*. *Handbook of Environmental Chemistry*.

Palter, J. B., Ames, E. J., Benavides, M., Goncalves Neto, A., Granger, J., Moisander, P. H., et al. (2020). High N_2 fixation in and near the Gulf stream consistent with a circulation control on diazotrophy. *Geophysical Research Letters*, *47*(16), e2020GL089103. https://doi.org/10.1029/2020GL089103

Pelegrí, J., & Csanady, G. (1991). Nutrient transport and mixing in the Gulf stream. *Journal of Geophysical Research*, *96*(C2), 2577–2583. https://doi.org/10.1029/90jc02535

Peng, X., Fawcett, S. E., van Oostende, N., Wolf, M. J., Marconi, D., Sigman, D. M., & Ward, B. B. (2018). Nitrogen uptake and nitrification in the subarctic North Atlantic Ocean. *Limnology & Oceanography*, *00*(4), 1462–1487. https://doi.org/10.1002/lno.10784

Ponsoni, L., Aguiar-González, B., Ridderinkhof, H., & Maas, L. (2016). The east madagascar current: Volume transport and variability based on long-term observations. *Journal of Physical Oceanography*, *46*(4), 1045–1065. https://doi.org/10.1175/JPO-D-15-0154.1

Poulton, A., Stinchcombe, M., & Quartly, G. (2009). High numbers of Trichodesmium and diazotrophic diatoms in the southwest Indian Ocean. *Geophysical Research Letters*, *36*, L15610. https://doi.org/10.1029/2009GL039719

Rafter, P., Bagnell, A., Marconi, D., & DeVries, T. (2019). Global trends in marine nitrate N isotopes from observations and a neural network based climatology. *Biogeosciences Discussions*. https://doi.org/10.5194/bg-2018-525

Rafter, P., DiFiore, P., & Sigman, D. (2013). Coupled nitrate nitrogen and oxygen isotopes and organic matter remineralization in the Southern and Pacific Oceans. *Journal of Geophysical Research: Oceans*, *118*(10), 47781–54794. https://doi.org/10.1002/jgrc.20316

Redfield, A., Ketchum, B., & Richards, F. (1963). *The influence of organisms on the composition of the Sea Water*. In M. Hill (Ed.), ed. : s.n., pp. 26–77.

Reid, J. (2003). On the total geostrophic circulation of the Indian Ocean: Flow patterns, tracers, and transports. *Progress in Oceanography*, *56*(1), 137–186. https://doi.org/10.1016/s0079-6611(02)00141-6

Ren, H., Chen, Y. C., Wang, X. T., Wong, G. T. F., Cohen, A. L., DeCarlo, T. M., et al. (2017). 21st-century rise in anthropogenic nitrogen deposition on a remote coral reef. *Science*, *356*(6339), 749–752. https://doi.org/10.1126/science.aal3869

Ren, H., Sigman, D., Thunell, R., & Prokopenko, M. (2012). Nitrogen isotopic composition of planktonic foraminifera from the modern ocean and recent sediments. *Limnology & Oceanography*, *57*(4), 1011–1024. https://doi.org/10.4319/lo.2012.57.4.1011

Ren, H., Sigman, D. M., Meckler, A. N., Plessen, B., Robinson, R. S., Rosenthal, Y., & Haug, G. H. (2009). Foraminiferal isotope evidence of reduced nitrogen fixation in the ice age Atlantic. *Science*, *323*(5911), 244–248. https://doi.org/10.1126/science.1165787

Richardson, P. (2007). Agulhas leakage into the Atlantic estimated with subsurface floats and surface drifters. *Deep-Sea Research Part 1*, *54*(8), 1361–1389. https://doi.org/10.1016/j.dsr.2007.04.010

Ridderinkhof, H., van der Werf, P. M., Ullgren, J. E., van Aken, H. M., van Leeuwen, P. J., & de Ruijter, W. P. M. (2010). Seasonal and interannual variability in the Mozambique Channel from moored current observations. *Journal of Geophysical Research*, *115*, C06010. https://doi.org/10.1029/2009JC005619

Ridgway, K., & Dunn, J. (2007). Observational evidence for a Southern Hemisphere oceanic supergyre. *Geophysical Research Letter*, *34*, L13612. https://doi.org/10.1029/2007GL030392

Roemmich, D., & Gilson, J. (2009). The 2004-2008 mean and annual cycle of temperature, salinity, and steric height in the global ocean from the Argo Program. *Progress in Oceanography*, *82*(2), 81–100. https://doi.org/10.1016/j.pocean.2009.03.004

Rohde, M., Granger, J., Sigman, D., & Lehmann, M. (2015). Coupled nitrate N and O stable isotope fractionation by a natural marine plankton consortium. *Frontiers in Marine Science*, *2*. https://doi.org/10.3389/fmars.2015.00028

Roman, R., & Lutjeharms, J. (2007). Red Sea intermediate water at the Agulhas current termination. *Deep-Sea Research I*, *54*(8), 1329–1340. https://doi.org/10.1016/j.dsr.2007.04.009

Roman, R., & Lutjeharms, J. (2009). Red Sea intermediate water in the source regions of the Agulhas current. *Deep-Sea Research I*, *56*(6), 939–962. https://doi.org/10.1016/j.dsr.2009.01.003

Russo, C., Lamont, T., Tutt, G., van den Berg, M., & Barlow, R. (2019). Hydrography of a shelf ecosystem inshore of a major western boundary current. *Estuarine, Coastal and Shelf Science*, *228*, 106363. https://doi.org/10.1016/j.ecss.2019.106363

Sarmiento, J., Gruber, N., Brzezinksi, M., & Dunne, J. (2004). High-latitude controls of thermocline nutrients and low latitude biological productivity. *Nature*, *427*(6969), 56–69. https://doi.org/10.1038/nature02127

Schmidt, G. A., Bigg, G. R., & Rohling, E. J. (1999). Global seawater Oxygen-18 Database-v1.22. https://data.giss.nasa.gov/o18data/

Schubert, R., Gula, J., Greatbatch, R. J., Baschek, B., & Biastoch, A. (2019). The submesoscale kinetic energy cascade: Mesoscale absorption of submesoscale mixed layer eddies and frontal downscale fluxes. *Journal of Physical Oceanography*, *50*(9), 2573–2589. https://doi.org/10.1175/JPO-D-19-0311.1

Shiozaki, T., Bombar, D., Riemann, L., Hashihama, F., Takeda, S., Yamaguchi, T., et al. (2017). Basin scale variability of active diazotrophs and nitrogen fixation in the North Pacific, from the tropics to the subarctic Bering Sea. *Global Biogeochemical Cycles*, *31*(6), 996–1009. https://doi.org/10.1002/2017GB005681

Shiozaki, T., Ijichi, M., Kodama, T., Takeda, S., & Furuya, K. (2014). Heterotrophic bacteria as major nitrogen fixers in the euphotic zone of the Indian Ocean. *Global Biogeochemical Cycles*, *28*(10), 1096–1110. https://doi.org/10.1002/2014GB004886

Shiozaki, T., Takeda, S., Itoh, S., Kodama, T., Liu, X., Hashihama, F., & Furuya, K. (2015). Trichodesmium and nitrogen fixation in the Kuroshio. *Biogeosciences*, *12*(23), 6931–6943. https://doi.org/10.5194/bgd-12-11061-2015

Siefert, R., Johansen, A., & Hoffmann, M. (1999). Chemical characterization of ambient aerosol collected during the southwest monsoon and intermonsoon seasons over the Arabian Sea: Labile-Fe(II) and other trace metals. *Journal of Geophysical Research*, *104*(D3), 3511–3526. https://doi.org/10.1029/1998JD100067

Sigman, D. M., Altabet, M. A., McCorkle, D. C., Francois, R., & Fischer, G. (1999). The $d^{15}N$ of nitrate in the Southern Ocean: Consumption of nitrate in surface waters. *Global Biogeochemical Cycles*, *13*, 1449–1166.

Sigman, D. M., Altabet, M. A., McCorkle, D. C., Francois, R., & Fischer, G. (2000). The $\delta^{15}N$ of nitrate in the Southern Ocean: Nitrogen cycling and circulation in the ocean interior. *Journal of Geophysical Research*, *105*(C8), 19599–19614. https://doi.org/10.1029/2000jc000265

Sigman, D. M., Casciotti, K. L., Andreani, M., Barford, C., Galanter, M., & Bohlke, J. K. (2001). A bacterial method for the nitrogen isotopic analysis of nitrate in seawater and freshwater. *Analytical Chemistry*, *73*(17), 4145–4153. https://doi.org/10.1021/ac010088e

Sigman, D. M., & Fripiat, F. (2019). Ocean process tracers: Nitrogen isotopes in the ocean. In J. Steele (Ed.), *Encyclopedia of ocean Sciences* (pp. 263–278). Academic Press.

Sigman, D. M., Granger, J., DiFiore, P. J., Lehmann, M. M., Ho, R., Cane, G., & van Geen, A. (2005). Coupled nitrogen and oxygen isotope measurements of nitrate along the eastern North Pacific margin. *Global Biogeochemical Cycles*, *19*(4). https://doi.org/10.1029/2005GB002458

Sigman, D. M., DiFiore, P. J., Hain, M. P., Deutsch, C., Wang, Y., Karl, D. M., et al. (2009). The dual isotopes of deep nitrate as a constraint on the cycle and budget of oceanic fixed nitrogen. *Deep Sea Research I*, *56*(9), 1419–1439. https://doi.org/10.1016/j.dsr.2009.04.007

Singh, A., Bach, L. T., Fischer, T., Hauss, H., Kiko, R., Paul, A. J., et al. (2017). Niche construction by non-diazotrophs for N_2 fixers in the eastern tropical North Atlantic Ocean. *Geophysical Research Letters*, *44*(13), 6904–6913. https://doi.org/10.1002/2017GL074218

Smart, S., Fawcett, S. E., Ren, H., Schiebel, R., Tompkins, E. M., Martinez-Garcia, A., et al. (2020). The nitrogen isotopic composition of tissue and shell-bound organic matter of Planktic foraminifera in Southern Ocean surface waters. *Geochemistry, Geophysics, Geosystems*, *21*(2), e2019GC008440. https://doi.org/10.1029/2019GC008440

Smart, S., Fawcett, S. E., Thomalla, S. J., Weigand, M. A., Reason, C. J. C., & Sigman, D. M. (2015). Isotopic evidence for nitrification in the Antarctic winter mixed layer. *Global Biogeochemical Cycles*, *29*(4), 427–445. https://doi.org/10.1002/2014GB005013

Smart, S., Ren, H., Fawcett, S. E., Schiebel, R., Conte, M., Rafter, P. A., et al. (2018). Ground-truthing the planktic foraminifer-bound nitrogen isotope paleo-proxy in the Sargasso Sea. *Geochimica et Cosmochimica Acta*, *235*, 463–482. https://doi.org/10.1016/j.gca.2018.05.023

Smith, J., Chavez, F., & Francis, C. (2014). Ammonium uptake by phytoplankton regulates nitrification in the Sunlit Ocean. *PLoS One*, *9*(9), e108173. https://doi.org/10.1371/journal.pone.0108173

Smith, S. (1984). Phosphorus versus nitrogen limitation in the marine environment. *Limnology & Oceanography*, *29*(6), 1149–1160. https://doi.org/10.4319/lo.1984.29.6.1149

Somes, C., Landolfi, A., Koeve, W., & Oschlies, A. (2016). Limited impact of atmospheric nitrogen deposition on marine productivity due to biogeochemical feedbacks in a global ocean model. *Geophysical Research Letters*, *43*(9), 4500–4509. https://doi.org/10.1002/2016gl068335

Souza, J., Montégut, C. D. M., Cabanes, C., & Klein, P. (2011). Estimation of the Agulhas ring impacts on meridional heat fluxes and transport using ARGO floats and satellite data. *Geophysical Research Letters*, *38*(21), L21602. https://doi.org/10.1029/2011GL049359

Stramma, L., & Lutjeharms, J. (1997). The flow field of the subtropical gyre of the South Indian Ocean. *Journal of Geophysical Research*, *102*(C3), 5513–5530. https://doi.org/10.1029/96jc03455

Straub, M., Sigman, D. M., Ren, H., Martinez-Garcia, A., Meckler, A. N., Hain, M. P., & Haug, G. H. (2013). Changes in North Atlantic nitrogen fixation controlled by ocean circulation. *Nature*, *501*(7466), 200–203. https://doi.org/10.1038/nature12397

Strickland, J., & Parsons, T. (1972). *A practical handbook of seawater analysis* (2nd ed.). Fisheries Research Board of Canada.

Takahashi, T., Sutherland, S. C., Wanninkhof, R., Sweeney, C., Feely, R. A., Chipman, D. W., et al. (2009). Climatological mean and decadal changes in surface ocean pCO_2 and net sea-air CO_2 flux over the global ocean. *Deep-Sea Research II*, *56*(8–10), 554–577. https://doi.org/10.1016/j.dsr2.2008.12.009

Talley, L. (2013). Closure of the global overturning circulation through the Indian, Pacific, and Southern Oceans: Schematics and transports. *Oceanography*, *26*(1), 80–97. https://doi.org/10.5670/oceanog.2013.07

Talley, L., Pickard, G., Emery, W., & Swift, J. (2011). *Descriptive physical Oceanography*. 6th ed. s.l.:Elsevier Ltd.

Thomas, L., Taylor, J., Ferrari, R., & Joyce, T. (2013). Symmetric instability in the Gulf stream. *Deep-Sea Research II*, *91*, 96–110. https://doi.org/10.1016/j.dsr2.2013.02.025

Toole, J., & Warren, B. (1993). A hydrographic section across the subtropical South Indian Ocean. *Deep-Sea Research Part I*, *40*(10), 1973–2019. https://doi.org/10.1016/0967-0637(93)90042-2

Voss, M., Bange, H. W., Dippner, J. W., Middelburg, J. J., Montoya, J. P., & Ward, B. (2013). The marine nitrogen cycle: Recent discoveries, uncertainties and the potential relevance of climate change. *Philosophical Transactions of the Royal Society; Biological Sciences*, *368*(1621), 20130121. https://doi.org/10.1098/rstb.2013.0121

Wada, E., & Hattori, A. (1976). Natural abundance of 15N in particulate organic matter in the north Pacific Ocean. *Geochimica et Comsochimica Acta*, *40*(2), 249–251. https://doi.org/10.1016/0016-7037(76)90183-6

Wallschuss, S., Mdutyana, M., Parrott, R. G., Forrer, H. J., Roman, R., Walker, D. R., et al. (2022). The influence of Agulhas leakage on primary production and nitrogen cycling in the southeastern Atlantic Ocean. *Journal of Geophysical Research: Oceans*, *127*(9), e2022JC018971. https://doi.org/10.1029/2022JC018971

Wang, W., Moore, K., Martiny, A., & Primeau, F. (2019). Convergent estimates of marine nitrogen fixation. *Nature Article*, *566*(7743), 205–211. https://doi.org/10.1038/s41586-019-0911-2

Wankel, S., Kendall, C., Pennington, J. T., Chavez, F. P., & Paytan, A. (2007). Nitrification in the euphotic zone as evidenced by nitrate dual isotopic composition: Observations from Monterey Bay, California. *Global Biogeochemical Cycles*, *21*(2). https://doi.org/10.1029/2006GB002723

Ward, B. (1985). Light and substrate concentration relationships with marine ammonium assimilation and oxidation rates. *Marine Chemistry*, *16*(4), 301–316. https://doi.org/10.1016/0304-4203(85)90052-0

Weber, T., & Deutsch, C. (2014). Local versus basin-scale limitation of marine nitrogen fixation. *Proceedings of the National Academy of Sciences of the United States of America*, *111*(24), 8741–8746. https://doi.org/10.1073/pnas.1317193111

Weigand, A., Foriel, J., Barnett, B., Oleynik, S., & Sigman, D. M. (2016). Updates to instrumentation and protocols for isotopic analysis of nitrate by the denitrifier method. *Rapid Communication in Mass Spectrometry: Protocol*, *30*(12), 1365–1383. https://doi.org/10.1002/rcm.7570

Wen, Z., Browning, T. J., Cai, Y., Dai, R., Zhang, R., Du, C., et al. (2022). Nutrient regulation of biological nitrogen fixation across the tropical western North Pacific. *Science Advances*, *8*(5). https://doi.org/10.1126/sciadv.abl7564

White, A., Granger, J., Selden, C., Gradoville, M. R., Potts, L., Bourbonnais, A., et al. (2020). A critical review of the $^{15}N_2$ tracer method to measure diazotrophic production in pelagic ecosystems. *Limnology and Oceanography: Methods*, *18*(4), 129–147. https://doi.org/10.1002/lom3.10353

Williams, R., & Follows, M. (2003). Chapter 2: Physical transport of nutrients and the maintenance of biological production. In M. Fasham (Ed.), *Ocean Biogeochemistry*, (pp. 19–51). s.l:Springer.

Williams, R., Roussenov, V., & Follows, M. (2006). Nutrient streams and their induction into the mixed layer. *Global Biogeochemical Cycles*, *20*(1). https://doi.org/10.1029/2005gb002586

Wong, A. (2005). Subantarctic mode water and Antarctic intermediate water in the South Indian Ocean based on profiling float data 2000–2004. *Journal of Marine Research*, *63*(4), 789–812. https://doi.org/10.1357/0022240054663196

Wu, C., Fu, F. X., Sun, J., Thangaraj, S., & Pujari, L. (2018). Nitrogen fixation by trichodesmium and unicellular diazotrophs in the northern South China Sea and the Kuroshio in summer. *Nature Scientific Reports*, *8*(1), 2415. https://doi.org/10.1038/s41598-018-20743-0

Wyrtki, K. (1971). *Oceanographic Atlas of the international Indian Ocean expedition*. National Science Foundation.

Yool, A., Martin, A., Fernández, C., & Clark, D. (2007). The significance of nitrification for oceanic new production. *Nature Letters*, *447*(7147), 999–1002. https://doi.org/10.1038/nature05885

Yu, L., & Weller, R. (2007). Objectively analyzed air-sea heat fluxes for the global ice-free oceans (1981-2005). *American Meteorological Society: Bulletin*, *88*(4), 527–539. https://doi.org/10.1175/bams-88-4-527

Zhang, R., Wang, X. T., Ren, H., Huang, J., Chen, M., & Sigman, D. M. (2020). Dissolved organic nitrogen cycling in the South China Sea from an isotopic perspective. *Global Biogeochemical Cycles*, *34*(12). https://doi.org/10.1029/2020GB006551